



**HAL**  
open science

## Mitochondrial Lon protease -depleted HeLa cells exhibit proteome modifications related to protein quality control, stress response and energy metabolism

Marie-Paule Hamon, Rachel Gergondey, Aurore L'Honoré, Bertrand Friguet

### ► To cite this version:

Marie-Paule Hamon, Rachel Gergondey, Aurore L'Honoré, Bertrand Friguet. Mitochondrial Lon protease -depleted HeLa cells exhibit proteome modifications related to protein quality control, stress response and energy metabolism. *Free Radical Biology and Medicine*, 2020, 148, pp.83-95. 10.1016/j.freeradbiomed.2019.12.039 . hal-02506939

**HAL Id: hal-02506939**

**<https://hal.sorbonne-universite.fr/hal-02506939>**

Submitted on 12 Mar 2020

**HAL** is a multi-disciplinary open access archive for the deposit and dissemination of scientific research documents, whether they are published or not. The documents may come from teaching and research institutions in France or abroad, or from public or private research centers.

L'archive ouverte pluridisciplinaire **HAL**, est destinée au dépôt et à la diffusion de documents scientifiques de niveau recherche, publiés ou non, émanant des établissements d'enseignement et de recherche français ou étrangers, des laboratoires publics ou privés.

**Mitochondrial Lon protease - depleted HeLa cells exhibit proteome modifications  
related to protein quality control, stress response and energy metabolism**

Marie-Paule Hamon, Rachel Gergondey, Aurore L'Honoré, Bertrand Friguet\*

Sorbonne Université, CNRS, INSERM, Institut de Biologie Paris-Seine, Biological Adaptation  
and Aging, B2A-IBPS, F-75005 Paris, France

\*Corresponding author:

Bertrand Friguet

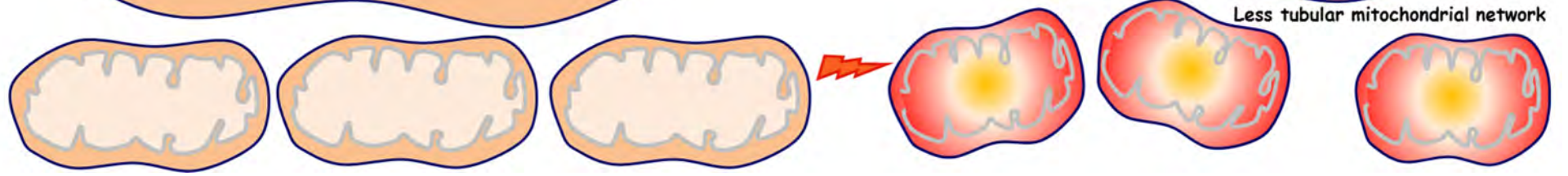
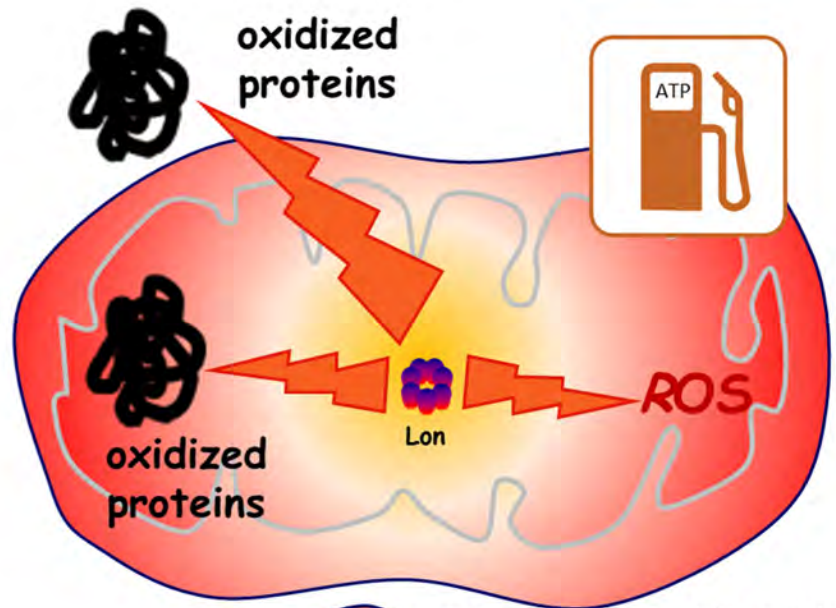
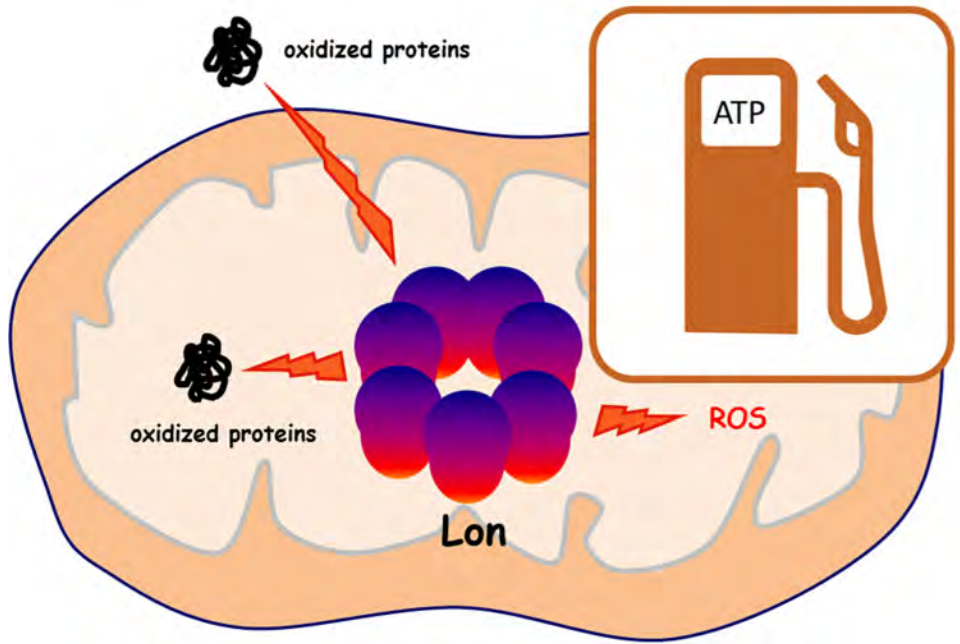
Sorbonne Université, CNRS, INSERM, Institut de Biologie Paris-Seine, Biological adaptation  
and Aging, B2A-IBPS, F-75005 Paris, France

Telephone: +33(0)144273702

E-mail: [bertrand.friguet@sorbonne-universite.fr](mailto:bertrand.friguet@sorbonne-universite.fr)

## **Highlights**

- Lon protease knockdown promotes oxidative stress and protein oxidation in HeLa cells
- Lon protease deficiency affects mitochondrial network morphology and cell proliferation
- Lon depletion impacts on stress response and energy metabolism protein expression
- Lon protease depletion decreases cell energy metabolic activity and ATP production



**Mitochondrial Lon protease - depleted HeLa cells exhibit proteome modifications  
related to protein quality control, stress response and energy metabolism**

Marie-Paule Hamon, Rachel Gergondey, Aurore L'Honoré, Bertrand Friguet\*

Sorbonne Université, CNRS, INSERM, Institut de Biologie Paris-Seine, Biological Adaptation  
and Aging, B2A-IBPS, F-75005 Paris, France

\*Corresponding author:

Bertrand Friguet

Sorbonne Université, CNRS, INSERM, Institut de Biologie Paris-Seine, Biological adaptation  
and Aging, B2A-IBPS, F-75005 Paris, France

Telephone: +33(0)144273702

E-mail: [bertrand.friguet@sorbonne-universite.fr](mailto:bertrand.friguet@sorbonne-universite.fr)

## **Abstract**

The ATP-dependent Lon protease is located in the mitochondrial matrix and oxidized proteins are among its primary targets for their degradation. Impairment of mitochondrial morphology and function together with apoptosis were observed in lung fibroblasts depleted for Lon expression while accumulation of carbonylated mitochondrial proteins has been reported for yeast and HeLa Lon deficient cells. In addition, age-related mitochondrial dysfunction has been associated with an impairment of Lon expression. Using a HeLa cell line stably transfected with an inducible shRNA directed against Lon, we have previously observed that Lon depletion results in a mild phenotype characterized by an increase of both production of reactive oxygen species and level of oxidized proteins (Bayot et al., 2014, *Biochimie*, 100: 38-47). In this study using the same cell line, we now show that Lon knockdown leads to modifications of the expression of a number of specific proteins involved in protein quality control, stress response and energy metabolism, as evidenced using a 2D gel-based proteomic approach and to alteration of the mitochondrial network morphology. We also show that these effects are associated with decreased proliferation and can be modulated by culture conditions in galactose versus glucose containing medium.

## **Key words**

Lon protease

HeLa cells

oxidative stress

proteomics

energy metabolism

mitochondrial dysfunction

**Running title:** Lon protease deficiency and proteome alteration

### **Abbreviations**

ABC, ammonium bicarbonate; ACN, acetonitrile; CHAPS, Cholamidopropyl)dimethylammonio]-1-propanesulfonate hydrate; ClpP, Clp protease proteolytic subunit; Cox2, cytochrome c oxidase subunit 2; DAPI, 4',6-diamidino-2-phenylindole; DFO, deferoxamine; 2-DG, 2-deoxy-D-glucose; DIGE, Differential Gel Electrophoresis; DMEM, Dulbecco's Modified Eagle Medium; DTT, Dithiothreitol; ECAR, extracellular acidification rate; EdU, 5-éthynyl-2'-déoxyuridine; FCCP, Carbonyl cyanide 4-(trifluoromethoxy)phenylhydrazone; Foxo3, Forkhead box protein O3; HEPES, 4-(2-hydroxyethyl)-1-piperazineethanesulfonic acid; Msrb2, Methionine-R-sulfoxide reductase B2; Nrf2, Nuclear factor erythroid 2-related factor 2; OCR, oxygen consumption rate; OXPHOS, oxidative phosphorylation; PBS, phosphate buffer saline; PCA, principal component analysis; RSLC, Rapid Separation Liquid Chromatographic; ROS, reactive oxygen species; shRNA, short hairpin RNA; tBH, tert-butyl-hydroperoxide; TCA, tricarboxylic acid cycle; TFA, TriFluoroAcetic acid; *TNF* tumor necrosis factor

### **Acknowledgments**

The authors wish to acknowledge Laurence Petit, Philippe Chaffey and Anne-Laure Bulteau for their help and advice concerning the flow cytometry, 2D DIGE experiments and the implementation of this study, respectively. The authors also thank the 3P5 proteomics facility, Université Paris Descartes, Sorbonne Paris Cité for the work performed for the proteomic and protein identification analyses.

### **Funding**

This research was supported by institutional funding from SU, CNRS and INSERM

## **Introduction**

Mitochondrial functions are various such as aerobic energy metabolism, regulation of intracellular calcium homeostasis, phospholipids and heme synthesis, contribution to cell growth and differentiation, cell cycle control and cell death. This broad repertoire includes ATP production by the respiratory chain for which mitochondria is often referred to as the powerhouse of the cell, a role that also makes it the main provider of intracellular reactive oxygen species (ROS) due to incomplete reduction of O<sub>2</sub> by the respiratory chain [1]. Although critical as signaling molecules when they are present at physiological levels [2], ROS can have detrimental effects when their production exceeds the antioxidant defense capacity, an imbalance that leads to oxidative injury involved in numerous diseases and in the aging process. Due to their close proximity with the respiratory chain, mitochondrial proteins are highly susceptible to oxidative damage. To counteract the deleterious effects of accumulation of damaged and misfolded proteins, mitochondria are equipped with quality control systems such as the Lon protease known to be a key player in the degradation of oxidized proteins [3] [4] [5].

First ATP-dependent protease being identified, Lon is located in the mitochondrial matrix where it is active as a homo-oligomeric ring complex. Each of its polypeptide chains contains both an AAA+ domain and a protease domain with a Ser-Lys catalytic dyad. Up to now, only another protease, called ClpP, has been identified in the mitochondrial matrix. While ClpP has been particularly involved in the mitochondrial unfolded protein response, Lon is active in degradation of oxidized proteins. Enzymes prone to oxidative damage are among its primary targets [5]. Both yeast and HeLa cells depleted for PIM1/Lon have been characterized by increased level of protein carbonylation [3], [6].

Thanks to its contribution to the mitochondrial quality control, Lon has a critical role in the maintenance of mitochondrial matrix protein homeostasis and hence in mitochondrial functional and structural integrity [7]. Thus, it was not surprising that impairment of



mitochondrial morphology and function and activation of apoptosis were observed in lung fibroblasts with Lon depletion [8]. Moreover, mitochondrial dysfunction reported in aged tissues or senescent cells has been associated with impairment of Lon protease expression and accumulation of oxidized mitochondrial proteins [9], [10]. The quality control activities of Lon are not restricted to degradation of modified protein and can also affect misfolded proteins and mitochondrial DNA [4]. Due to the emerging role of the Lon protease as an important regulator of mitochondrial functions [11], it is expected that Lon down-regulation impairs several mitochondrial activities with an impact on cellular functions.

To investigate this hypothesis, we used a previously described transgenic HeLa cell line that can inducibly express Lon shRNA when treated with doxycycline [6]. Using a 2D DIGE proteomic approach, we show that the mild oxidative stress induced by Lon depletion is correlated with an altered expression pattern of proteins involved in several cellular pathways such as energy metabolism, protein quality control and stress response. In agreement with these results, we then demonstrate that loss of Lon in HeLa cells affects their metabolic activity with negative consequences on both ATP production and cell proliferation. Interestingly, we show that most of these effects, that are indicative of mitochondrial dysfunction, can be modulated by culture conditions.

## **Material and methods**

### ***Materials and cells***

All reagents were purchased from Sigma (Sigma Aldrich, St. Louis, MO, USA) unless otherwise stated. HeLa T-Rex cells were transfected as previously reported [6] with a 68-base Lon-specific oligonucleotide (50-gatctccgttcgtctcgcccagccttttcaagagaaaggctgggcgagacgaacttttgaaagctt-30) annealed to its complementary sequence pENTR/H1/T0+ (Block it-Invitrogen) and inserted into pENTR/H1/T0+ (Block it-Invitrogen). For the glucose containing medium condition, clones of HeLa-tet-on-shLon cells were cultivated in Dulbecco's Modified Eagle's Medium (DMEM, Gibco Life Technologies, Carlsbad, CA, USA) with 5mM glucose. For the galactose containing medium condition, clones of HeLa-tet-on-shLon cells were cultivated in DMEM (Gibco Life Technologies) with 5mM galactose and 1mM pyruvate. Both media were supplemented with 10% fetal bovine serum, 5 mg/ml blasticidin (Invitrogen), 200 mg/ml zeocin (Invitrogen), with (Dox+) or without (Dox-) 2 µg/ ml doxycycline.

### ***Mitochondrial morphological analysis***

For immunofluorescent labeling of the mitochondrial compartment, cells were plated at subconfluence on glass coverslips in different conditions: 2.5 days in DMEM + 5mM glucose, 1.5 day in DMEM + 1mM pyruvate and 5mM galactose, 20 hours in DMEM + 1mM pyruvate and 10mM déoxyglucose, 20 hours in DMEM + 5mM glucose with 1µg/ml oligomycin, 3 hours in DMEM + 5mM glucose with 250µM tert-butyl-hydroperoxide, 3 days in DMEM + 5mM glucose and 3% oxygen in a Baker Ruskinn SCI-tive hypoxia workstation, 1 day in DMEM + 5mM glucose with 100µM deferoxamine (DFO). After fixation (4% paraformaldehyde, 0.1% glutaraldehyde), the mitochondrial compartment was visualized by immunofluorescence using

polyclonal antibody directed against cytochrome c oxidase subunit 2 (Anti-MTCO2 Abcam ab91317) and then *anti-rabbit* IgG (H+L) secondary antibody Alexa Fluor® 568. The coverslips were mounted in Fluoroshield mounting medium (Sigma) containing 0.15µg/mL DAPI. Fluorescent images were acquired using Zeiss microscope (Zeiss, Jena, Germany) and processed with Motic Images Advance 3.2. Quantitative analysis of mitochondrial morphology (area and perimeter) was performed according to the protocol described by Koopman et al [12] using ImageJ software. 30 individual cells were analyzed per cover slip and the aspect ratio (AR), that represents mitochondrial elongation, was calculated for each condition.

#### ***Mitochondrial ROS evaluation with flow cytometry***

Mitochondrial superoxide anion production was monitored using MitoSOX™ Red 5µM (Molecular probes, Courtaboeuf, France). Cell fluorescence was quantified by flow cytometry using MACSQuant VYB.

#### ***Proliferation Assay***

Cell proliferation was quantified by EdU incorporation (10 µM for 15 min in cell culture media). For EdU detection, the Click-iT EdU Cell Assay kit (Invitrogen) was used following the manufacturer's instructions.

#### ***Cellular ATP assay***

Cellular ATP levels were determined using CellTiter-Glo® Luminescent Assay (Promega, Madison, WI, USA) according to the manufacturer's instructions.

### ***Preparation of mitochondrial fractions***

For preparation of mitochondria-enriched fractions, cells were harvested and resuspended in HEPES-sucrose buffer (Hepes 10mM sucrose 250mM, pH 7.4). All the subsequent steps were carried out at 4° C. Cells were homogenized and then passed through a 22G needle. Membranes and nuclear fractions were removed by centrifugation at 1000 g for 5 min and supernatants were centrifuged (11000 g, 10 min, 4°C). Mitochondrial fraction present in the pellets was immediately used for protein extraction or frozen.

### ***Protein extracts***

For whole cell extracts, cells were harvested and lysed in Cell Lytic M (Sigma Aldrich C2978) according to the manufacturer's instructions.

Protein content of whole cell and mitochondrial fractions were determined using the Bradford protein assay (Bio-Rad, Marnes la Coquette, France), with bovine serum albumine as a standard.

### ***Detection of carbonylated proteins***

Carbonylated proteins were detected and analyzed after labeling of protein carbonyl groups with CF647DI hydrazide (Biotium, Fremont, CA, USA) for 45 min at room temperature under medium agitation. Labeled samples were resolved by SDS-PAGE in Any-KD precast gels (Bio-Rad). After three washes in 7% acetic acid/10% ethanol, gels were scanned with Ettan DIGE Imager (GE Healthcare, Saclay, France).

### ***Western blotting***

Proteins were separated by SDS-PAGE using Biorad Any-KD precast gels and electro-transferred onto Hybond nitrocellulose membrane (GE Healthcare). Primary antibodies used were anti-CLPP (Abcam ab124822), anti-MSRB2 (Abcam ab101513), anti-FKHRH-144

(Santa Cruz Biotechnology, Dallas, TX, USA, sc-11351), anti-NRF2 (Santa Cruz Biotechnology, sc-365949), and anti Lon prepared as previously described [13]. After overnight incubation at 4°C in PBST/milk 5% or PBST/Sea block Blocking buffer (37527 Thermo Fisher Scientific, Courtaboeuf, France ), primary antibodies were detected using peroxidase-conjugated secondary antibodies (Bio-Rad) or goat anti-rabbit IgG (H+L) Cross-Adsorbed Secondary Antibody, Dy Light 800 (Invitrogen). Quantification of western blot signals was performed using the ImageJ software.

### ***2D DIGE proteomic analysis***

Frozen mitochondria pellets were resuspended and homogenized in lysis buffer (8M urea, 2M thiourea, 4% CHAPS, 60mM DTT). Then the protein extracts were clarified by ultracentrifugation at 100000g for 1 h at 4°C. Samples were treated with the 2D Clean-Up kit (GE Healthcare) according to the manufacturer's instructions. The resulting dry pellets were resuspended in lysis buffer (8M urea, 2M thiourea and 4% CHAPS) and adjusted to pH 8.5 with 1.5M Tris-base. After lysates clarification by centrifugation at 20 000g for 15 min at 4°C, protein concentrations of the supernatants were determined by the Bradford method, and were in the range of 6–10µg/µL.

For 2D DIGE experiment, protein labelling with CyDyes<sup>TM</sup>Fluor minimal dyes (GE Healthcare) and 2D-electrophoresis were done as previously described [14] using 50µg mitochondrial extracts.

Image analysis, relative quantification and statistical evaluation were carried out using DeCyder<sup>TM</sup> 2D software (GE Healthcare, version 7.2). The fold change (FC) and Student's t-test p-values were calculated across pairwise comparisons (glucose Dox- vs glucose Dox+; galactose Dox- vs galactose Dox+) and considered significant for p values < 0.05 and FC ≥1.3 or ≤1.3. Spots of interest were identified for protein content by mass spectrometry.

### ***Mass spectrometry***

In-gel digestion was carried out with trypsin, according to previously published procedure with minor modifications [15]: samples were destained twice with a mixture of 100mM ammonium bicarbonate (ABC) and 50 % (vol/vol) acetonitrile (ACN) for 45 min at room temperature. After dehydration using 100 % ACN for 15 min, samples were reduced with 25mM ABC (10mM DTT) for 1 h at 57 °C and alkylated (55mM iodoacetamide in 25mM ABC) for 30 min in the dark at room temperature. Gel pieces were washed twice with 25mM ABC, dehydrated twice with 100% ACN (15 min each) and dried (20 min). Gel cubes were incubated with sequencing grade-modified trypsin (Promega; 12.5 ng/μl in 40mM ABC with 10% ACN, pH 8.0) overnight at 37 °C. After digestion, peptides were extracted twice from gel pieces, first with a mixture of 50 % ACN – 5 % formic acid (FA) and second with 100% ACN. All these steps were done with a robot (Tecan, Mannedorf, Switzerland). Extracts were then dried using a vacuum centrifuge concentrator plus (Eppendorf, Hamburg, Germany).

Mass spectrometry analyses were performed using an Ultimate 3000 Rapid Separation Liquid Chromatographic (RSLC) system (Thermo Fisher Scientific) online with a Q Exactive Plus hybrid quadrupole Orbitrap mass spectrometer (Thermo Fisher Scientific). Briefly, peptides were solubilized in 3.5 μL of 10 % ACN - 0.1 % TriFluoroAcetic acid (TFA). Then, peptides were loaded and washed on a C<sub>18</sub> reverse-phase precolumn (3 μm particle size, 100 Å pore size, 75 μm i.d., 2 cm length). The loading buffer contained 98% H<sub>2</sub>O, 2% ACN and 0.1% TFA. Peptides were then separated on a C<sub>18</sub> reverse-phase resin (2 μm particle size, 100 Å pore size, 75 μm i.d., 25 cm length) with a 20 min gradient from 99 % A (0.1 % TFA and 100 % H<sub>2</sub>O) to 50 % B (80 % ACN, 0.085 % TFA and 20% H<sub>2</sub>O).

The mass spectrometer acquired data throughout the elution process and operated in a data-dependent scheme with full MS scans acquired with the Orbitrap, followed by up to 10 MS/MS HCD spectra in the Orbitrap. Mass spectrometer settings were: full MS (AGC:  $3 \times 10^6$ ,

resolution:  $7 \times 10^4$ ,  $m/z$  range 400–2000, maximum ion injection time: 100 ms) and MS/MS (AGC:  $1 \times 10^5$ , maximum injection time: 100 ms, isolation window: 4 $m/z$ , dynamic exclusion time setting: 15 s). The fragmentation was permitted for precursors with a charge state of 2, 3 and 4. For the spectral processing, the software used to generate .mgf files was Proteome discoverer 1.4. Database searches were carried out using Mascot version 2.5.1 (Matrix Science, London, UK) on ‘human’ proteins (20,273 sequences) from the SwissProt databank containing 550 552 sequences (196 472 675 residues) (February 2016). The search parameters were as follows: the enzyme specificity as trypsin, carbamidomethylation as a variable modification for cysteins and oxidation as a variable modification for methionines. Up to 1 missed cleavage was tolerated, and mass accuracy tolerance levels of 4 ppm for precursors and 20 mmu for fragments were used for all tryptic mass searches. Positive identification was based on a Mascot score above the significance level (i.e. 5%). The reported proteins were always those with the highest number of peptide matches. Analysis, integration and interpretation of proteomic data derived from this 2D DIGE were performed with the Ingenuity Pathway Analysis software.

### ***Seahorse metabolic analysis***

Oxygen consumption rate (OCR) and extracellular acidification rate (ECAR) were analyzed on a Seahorse XFe24 extracellular flux analyser (Seahorse Biosciences, North Billerica, MA, USA) according to the manufacturer's instructions. Briefly, control and mutant cells were seeded at a density of 80 000 cells per well in a Seahorse XF24 plate and cultured for 12 hrs. The seeding density was based on initial assays that optimized both OCR and ECAR. One hour before the assay, cultured cells were washed three times in DMEM minimal assay media (Seahorse Biosciences, 37 °C, pH 7.40) supplemented with 1mM pyruvate and 2mM glutamine for ECAR measurements and with 5mM glucose or 5mM galactose for OCR essays, and equilibrated for 1 h at 37 °C in a non-CO<sub>2</sub> incubator. OCR and ECAR were measured in control

condition (basal rates) and after successive injections of oligomycin 1 $\mu$ M, FCCP 1 $\mu$ M and rotenone 10 $\mu$ M for OCR measurements, and 5mM glucose or 5mM galactose, 1 $\mu$ M oligomycin and 100 $\mu$ M 2 deoxy-D-glucose for ECAR measurements. At the end of the experiment, proteins were extracted using 10 $\mu$ l of lysis buffer and quantified using the Bradford assay. OCR and ECAR values were then normalized to protein concentration in order to compare different conditions.

### ***Statistical analysis***

Results are presented as mean  $\pm$  SEM. Differences between two groups were assessed by Student's t-test or Mann-Whitney test for non Gaussian distributions. Comparisons between more than two groups were assessed using one-way Anova test or Kruskal-Wallis test for non Gaussian distributions. Principal component analysis (PCA) was performed using the DeCyder software. PCA is a mathematical procedure that can convert a set of variables (here proteome maps) into a coordinate system so that the greatest variance is depicted on the first coordinate (called first component or PC1), the second greatest variance on the second coordinate (PC2).



## Results

### *Lon depletion is generally associated with a more fragmented mitochondrial network and increased carbonylated protein level and mitochondrial superoxide production*

Since the Lon protease has been characterized as a stress responsive protein [16], we first examined the effects of three metabolic settings, namely galactose, 2-Deoxy-D-glucose (2-DG), oligomycin, of tert-butyl-hydroperoxide (tBH) [17] for its oxidant properties, and of two hypoxic conditions, i.e. upon 3% oxygen and using deferoxamine (DFO), on mitochondrial dynamics and protein carbonylation of control and Lon-depleted cells. Both are interesting informers regarding stress. Indeed, the first one can be considered as an early sign of cellular stress [18] while the second one is a major indicator of protein oxidative damage [19] against which Lon is especially effective [20], [21].

Due to the importance of the appearance of the mitochondrial network in revealing the status of mitochondria, we investigated mitochondrial dynamics, and more specifically changes in mitochondrion length, using the aspect ratio (AR) defined by Koopman et al [12]. In basal conditions (glucose), Lon-depleted cells are characterized by a reduced AR factor compared to control cells, revealing an increased fragmentation of the mitochondrial network (Fig 1A & B). We then treated control and Lon-knockdown cells with four chemical stressors in order to investigate the effect of Lon depletion in these conditions. Two carbon sources (i. e. glucose and galactose) and low oxygen (i.e. 3%) cell culture condition were also used. Results, presented in figure 1A and B, show that Lon depletion markedly increases mitochondrial fragmentation when cells are cultured in galactose condition but only slightly affects the mitochondrial network in response to 2-DG, oligomycine, tBH, 3% oxygen and DFO treatments. Interestingly, 3% oxygen is the only condition associated with a slightly more interconnected mitochondrial network upon Lon down-regulation. Although DFO is often used as a hypoxia-

mimicking agent [22], no significant change in mitochondrial network morphology is observed upon treatment with this iron chelator in a context of Lon depletion.

We have previously reported that Lon depletion in HeLa cells is associated with an increase of oxidatively modified proteins when cells are cultured with glucose as carbon source [6]. Using protein carbonyls as a marker of irreversible protein oxidation [23], Lon-depleted cells (Dox+) showed significant increase in protein carbonylation compared to control cells (Dox-) when cultured in glucose condition (Fig 1C & D). This phenotype is similar when cells are cultured in presence of galactose and the same trend is also observed with tBH (Fig 1D). In contrast, treatments with 2-DG and oligomycin, that are inhibiting glycolysis or mitochondrial respiration respectively, did not result in increased protein oxidation either in control or in Lon-depleted cells. Similar observations or, on the contrary, increased oxidative stress have already been noted with both reagents [24], [25], [26], [27], [28], [29]. Concerning the 3% oxygen and the hypoxia-mimetic DFO treatments, Lon knockdown is associated with no significant change in protein carbonylation in the first case and with more carbonylated proteins in the second case. Taken together, these results are in accordance with a more fragmented mitochondrial network being a predominant morphological state during elevated stress [30].

Interestingly, replacing glucose by galactose to promote mitochondrial respiration, induced the most important increase in mitochondrial network fragmentation (Fig 1A) as well as elevated levels of protein carbonylation (Fig 1C) in Lon-depleted cells as compared to control cells. These results led us to further investigate the effects of Lon depletion with HeLa cells cultured in galactose versus glucose containing medium.

To address the effects of Lon depletion on mitochondria oxidative status, we measured mitochondrial superoxide production (Fig 1E) and carbonylated proteins levels (Fig 1F). Results, presented in figure 1E and F, show that Lon knockdown is associated with an increase in each parameter, in both glucose and galactose conditions. Regarding the increase in ROS

and carbonylation levels in galactose compared to glucose medium, these results are consistent with those found when galactose was used to instigate aging in various models [31].

### ***Lon depletion affects mitochondrial protein maintenance in galactose and glucose containing medium***

We then investigated whether other mitochondrial proteases or repair proteins may compensate for Lon depletion. We focused on two proteins, namely ClpP, the second other protease localized in the mitochondrial matrix, and MsrB2 involved in oxidized protein repair, [4] [32]. Results, presented in figure 2, show a significant up-regulation of MsrB2 expression in both glucose and galactose conditions (Fig 2A), together with an increased ClpP level in galactose (Fig 2B). These results demonstrate that Lon depletion, by the increase of mitochondrial ROS production and accumulation of carbonylated proteins, leads to cell compensation through up-regulation of ClpP and MsrB2 expression, with a more important response in galactose containing medium.

### ***Lon depletion leads to increased expression of mitochondrial proteins***

To fully explore protein expression modifications arising with Lon deficiency, we then investigated the consequences of Lon depletion on cell proteome using the 2D DIGE technology. Four mitochondria-enriched fractions of each condition (glucose Dox-, glucose Dox+, galactose Dox-, galactose Dox+) were compared, with each condition being labeled with an individual CyDye (Fig 3A). After electrofocusing and migration, gels were analyzed with DeCyder. The Principal Component Analysis (PCA) grouped together the samples belonging to the same category (Fig 3B) revealing that each group have its own profile determined by both expression level of the Lon protease and culture medium. In glucose condition, mass spectrometry of selected spots analysis resulted in the identification of 78 proteins, the

expression of which is altered when Lon is depleted. Among them, 43 proteins are overexpressed, with more than 50% being previously described in mitochondria (Table 1). In contrast, among the 35 proteins that exhibit a down-regulated expression, less than 20% are localized in mitochondria (Table 2). Similar results were obtained when cells are cultured in presence of galactose (Tables 3 & 4), suggesting that Lon depletion leads to increased expression levels of proteins localized in mitochondria.

***Lon depletion results in altered expression of proteins involved in quality control and stress response and in energy metabolism***

We then investigated the consequences of Lon depletion on cellular pathways. A first global analysis using DeCyder revealed that whatever the glucose or galactose condition, more than 50% of the proteins the expression of which is affected by Lon depletion are involved in stress response and protein quality control or in bioenergetic pathways. A second analysis, using the Ingenuity Pathway Analysis software showed that, in glucose medium (Fig 4A), proteins with modified expression notably act in four fields of the stress response and protein quality control, namely (1) stress response (PHB, YWHAE/14-3-3 protein epsilon), (2) apoptosis (Diablo, HtrA2), (3) NADH/NAD<sup>+</sup> regulation (HSD17B10, DLD) and (4) chaperone activity (HSPD1/Hsp60, the tandem Hsp70-Hsp90 and the PI3Kinase complex). Interactions between the PI3K complex and Hsps have been previously demonstrated [33], [34]. In galactose medium three of these four fields are affected by a Lon deficiency (Fig 4B).

As both 14-3-3 protein epsilon and PI3kinase have been involved in regulation of Foxo and Nrf2 signaling pathways, we then investigated the expression levels of these two transcription factors inducible by oxidative stress [35], [36]. Western-blot results presented in figure 5 show that, in glucose medium, FoxO3 expression decreased (Fig 5A) while Nrf2 expression is slightly up-regulated by Lon depletion (Fig 5B). These results are consistent with the

overexpression of 14-3-3 protein epsilon and PI3K. Indeed, downstream of PI3K, active AKT phosphorylates FoxO transcription factors generating binding points for 14-3-3 proteins which block FoxO DNA binding and accelerate its nuclear export while inhibiting import [37], [38]. Conversely, PI3K can promote the translocation of Nrf2 to the nucleus where it can activate the antioxidant response genes expression [39].

Analysis of the 2D DIGE experiment also revealed modifications of energy metabolism pathways, with a decreased expression of five and three glycolytic enzymes in glucose and galactose conditions respectively (Fig 6A). Oxidative phosphorylation is mainly impacted by the overexpression of components of complexes I, III and V. Still in mitochondria, other energy metabolism pathways are also impacted such as gluconeogenesis, TCA cycle, fatty acid  $\beta$ -oxidation, lipid synthesis and urea cycle (Tables 1 to 4 in supplementary data).

As observed for quality control and stress response, the number of proteins involved in energy metabolism and showing modified expression upon Lon depletion was also more important in glucose compared to galactose containing medium (Fig 4A & B; Fig 6A & B).

### ***Lon depletion results in alterations of the energetic metabolism***

In view of these proteomic results focusing on energy metabolism, we next performed functional studies using the Seahorse analyzer to assess the contribution of the mitochondrial respiratory chain and glycolysis to the energetic status of Lon-depleted cells. In both glucose and galactose conditions, Lon-depleted cells exhibited reduced metabolic activity both in terms of oxygen consumption (OCR) and extracellular acidification (ECAR) (Fig 7A & B). Considering the ratio OCR versus ECAR as a measure of the relative magnitude of OXPHOS versus glycolysis, Lon-depleted cells in glucose exhibited a higher preference for glycolysis (Fig 7C). As expected, HeLa cells in galactose demonstrated a reduced glycolytic activity compared to glucose condition, (Fig 7A) but, surprisingly, this decline was not compensated

by an increase of OXPHOS activity (Fig 7B).

Concerning the cellular responses to drugs injections performed during the Seahorse metabolic analyzer experiments, Lon-depleted cells presented a decreased productivity in term of OCR (basal respiration, ATP linked respiration, maximal respiratory capacity and reserve respiratory capacity) except for proton leak respiration (Fig 7D to H). This last observation is in accordance with the increase of mitochondrial ROS production that is observed in Lon-depleted cells and that is known to activate proton leak [40] [41]. This stimulation may minimize oxidative damage by tempering electrical potential and mitochondrial superoxide production [42].

Regarding glycolytic activities measured with ECAR, glycolytic capacity is the only declining parameter when Lon is knocked down (Fig 7J). Lon-depleted cells in glucose exhibit no modifications of their basal glycolysis (Fig 7I) but the lowest reserve respiratory capacity (Fig 7G) that may be related with their more glycolytic profile (Fig 7C).

Taken together, all these results show that Lon depletion leads to mitochondrial network fragmentation, increased ROS and protein carbonylation levels and altered energetic metabolism, revealing a mitochondrial dysfunction.

### ***Lon depletion differentially affects HeLa cells proliferation and ATP levels in galactose versus glucose containing medium***

In view of the consequences of Lon depletion on mitochondria, we then investigated whether it could also impact cell survival or proliferation. Analysis of their proliferation revealed a marked decrease in the number of EdU-positive cells compared to control cells (Fig 8A & B). This decline is not observed in glucose condition, but only when cells are cultured in galactose, as already reported for cancer cells in this medium [43] [44]. This result is correlated with the reduction of the glycolytic capacity noted in Lon-depleted cells in galactose, and suggests an altered ATP production. As expected, Lon-depleted cells exhibit a marked reduction of their

ATP levels (Fig 8C), a phenotype that could account for the reduction of their proliferative capacity. Taken together, these results indicate that in HeLa cells, Lon protease is critical for the maintenance of mitochondrial function, and as a consequence, for cell proliferation. In its absence, HeLa cells exhibit altered expression of quality control and stress response pathways and altered energy metabolism leading to increased ROS and carbonylation levels and to a reduced proliferation.

## **Discussion**

In this study, we have investigated the effects of Lon depletion on protein and redox homeostasis as well as mitochondrial function in different metabolic conditions and stress situations. The observed mitochondrial network fragmentation and increase in carbonylated protein levels generally concomitant with Lon knockdown (Fig 1) validates the important role of this mitochondrial protease in protein homeostasis, particularly when it comes to oxidative stress [20]. Variations of mitochondria morphology were previously observed in human lung fibroblasts with a Lon depletion on the basis of criteria that differ from the quantitative AR factor used here [8].

Mitochondrial network modifications associated with Lon deficiency (Fig 1A) support a deleterious effect of Lon down-expression. Mitochondrial dynamics is a part of quality control systems as fusion allows mitochondria to compensate defects in some of them while fission segregates healthy from damaged mitochondria when a certain threshold of damage is reached [45]. Fragmentation predominantly observed here with Lon down-regulation can thus indicate a mitochondrial dysfunction that appears more important in galactose than in glucose. Furthermore oxidative phosphorylation deficiency has been previously proven to be responsible for mitochondrial fragmentation [46]. A mitochondrial dysfunction was also found in Lon-depleted melanoma cells that displayed an increase in mitochondrial fragmentation and ROS production, which caused the proteolytic processing of OPA1 [47]. Indeed, an excessive OPA1 processing can also promote mitochondrial fragmentation [48]. Concerning the network elongation exhibited by control cells in galactose and 2-DG, this has already been reported in HeLa cells upon glucose deprivation [43] [49]. This is most likely due to a switch from anaerobic to aerobic energy production, an adaptative response accompanied by a more extended mitochondrial network [50].



Different parameters must be taken into account regarding the slight mitochondrial network elongation observed in a hypoxic environment, i.e. with 3% O<sub>2</sub>. HeLa cells originated from a human cervical cancer and exposition of cancer cells to long-term hypoxia, as it is the case with 3% O<sub>2</sub> during 72 hours, can induce mitochondrial fusion in order to evade apoptosis in a HIF-1 dependent manner [51]. It is also with the aim of avoiding cell death that HeLa cells are responding to a redox stress with a fusion mechanism [52]. That may explain why Lon-depleted cells have more elongated mitochondrial network when submitted to 3% O<sub>2</sub> (Fig 1A and B). It is also possible that the triggered expression of Lon previously reported upon hypoxia [53] [54] [55] has partly offset the Lon knockdown. Furthermore, this mitochondrial elongation can result from a Keap1-Nrf2 stress response pathway [56] given that an enhanced Nrf2 expression (Fig 5B) is observed when Lon is down-regulated.

Interestingly, it is with DFO that the most important increase in protein carbonylation was observed in Lon-depleted cells (Fig 1 C and D). Indeed, beside the mitochondrial dysfunction that could be induced by this reagent, DFO has also demonstrated oxidant capacities [57] [58] [59] that may contribute to the oxidized protein build-up observed in the absence of Lon (Fig 1A and B). In contrast, together with the elongated mitochondrial network, the absence of increased protein carbonylation noted in Lon-depleted cells grown under 3% O<sub>2</sub> (Fig 1C) confirm that cells adapt here to hypoxia using a different strategy, probably by decreasing ROS levels as previously reported in human fibroblasts [60].

Relevant with the efficiency of Lon protease in eliminating oxidized proteins, high levels of carbonylated proteins was also observed upon Lon depletion and tBH induced oxidative stress (Fig 1D). Concerning the different metabolic conditions with 2-DG and oligomycin, they did not seem to impose on Lon-depleted cells more oxidative injury than in glucose condition. Important levels of protein carbonylation in both control and Lon-depleted cells were obtained

with galactose (Fig 1C) which is consistent with galactose propensity to promote aging in some animal models [61] particularly through increased oxidative stress [62].

Based on the network morphology and the oxidative status of the Lon-depleted cells, we can propose, except when cells are grown under 3% O<sub>2</sub>, that Lon knockdown has created a stressful condition that could affect mitochondrial function. This observation appeared to be underlined by mitochondrial quality control actors since a proteotoxic stress response arose in Lon-depleted cells from MsrB2 (Fig 2B) and, in a lesser extent, the ClpP protease (Fig 2A). Concerning the decreased expression of FoxO3 in cells with galactose and upon Lon depletion (Fig 5A), this has already been found in aging cells and animals [63] [61]. The signaling pathway response may rather come from Nrf2 (Fig 5B), well-known for its role in antioxidant defense, particularly in the case of threatened mitochondrial homeostasis [36], even if galactose treatment reduced Nrf2 protein levels in mice [64]. Moreover, a binding site for Nrf2 was found on the Lon promoter in a region essential for up-regulating Lon in the presence of oxidative stress [65].

Analysis of the 2D DIGE results confirmed that stress response and protein quality control were particularly affected by Lon depletion (Fig 3C and tables 1 to 4 in supplementary data). In particular, without Lon, another mitochondrial serine protease showed enhanced expression, i.e. HtrA2 (Fig 4 area 2), which is known for acting in case of oxidative stress [66]. Also overexpressed when Lon is down-regulated, prohibitins (Fig 4 area 1) have been reported to play a role in protecting against oxidative stress [67]. Concerning the modified expression of dehydrogenases found in Lon-depleted cells (Fig 4 area 3), their potential effect on the NAD/NADH ratio may also influence the oxidative status [68].

2D DIGE results also revealed modified expression of numerous proteins involved in energy metabolism. Down-regulated proteins upon Lon depletion are essentially located in cytosol and implicated in glycolysis (Fig 6A). A down-expression of enzymes involved in glycolysis has

been previously found in muscle of old women with decreased energy metabolism [69]. Moreover, inhibition of enzymes of glycolysis can be a strategy to combat oxidative stress [70]. Up-regulated proteins are rather situated in the mitochondria and involved in OXPHOS (tables 1 to 4 in supplementary data), (Fig 6B). Such a transcriptional activation of proteins involved in the composition, functioning and assembly of respiratory chain has already been reported in response to mitochondrial OXPHOS deficiencies [71]. In glucose condition, this remodeling is accompanied by overexpression of  $\beta$ -oxidation components and reduced levels of lipid synthesis related proteins. A similar metabolic reorganization has already been reported in cancer cells [72] and obesity-resistant mice [73] showing decreased lipid biosynthesis and increased lipid utilization in the mitochondria through fatty acid oxidation. This could counterbalance the reduced glycolysis and OXPHOS activities observed with Lon depletion (Fig 7A, B) through increased production of lipolytic products and down-regulation of lipid/sterol synthetic pathways.

Reduced energy metabolic activity noted in Lon-depleted cells (Fig 7A & B) confirmed the hypothesis of mitochondrial dysfunction related to Lon deficiency and more importantly in galactose medium. This is consistent with the fall in ATP levels observed in Lon-depleted cells (Fig 8C). Lon-depleted cells revealed less active energy metabolic activity for most parameters measured in this study (Fig 7D to K). Such an hypometabolism has been noted in a mouse model of Alzheimer's disease exhibiting oxidative stress and mitochondrial dysfunction [74]. Among the parameters that can indicate mitochondrial anomalies are respiratory reserve (Fig 7G), the exhaustion of which has been reported with altered mitochondrial function [75], and decreased glycolytic reserve (Fig 7K) also indicating less tolerance to metabolic stress.

Oxidative stress has been shown to inhibit glycolysis [76] and to impair oxidative phosphorylation [77]. Due to the complex interplay between protein oxidative damage and energy metabolism defect, it is not easy to determine how each of them shares the responsibility

of the decline of mitochondrial function observed here. Actually a decline of mitochondrial function is found in numerous diseases and the aging process [78]. Decreased mitochondrial respiration can also be an adaptive stress response to face a redox stress [79] as well as reduced flux of the lower part of glycolysis [80]. It was mainly in this part of glycolysis that we found a down-regulation of some glycolytic enzymes when Lon is depleted.

At the cellular level, the mitochondrial dysfunction observed with Lon depletion is associated with reduced ATP levels (Fig 8C), and decreased proliferation in galactose medium (Fig 8A & B). In galactose, energy metabolism is more dependent on oxidative phosphorylation [81] [82]. Hence the mitochondrial failure linked to Lon knockdown is more pronounced in galactose condition that cumulates the decreased ATP production and proliferative capacity as noted in cells with OXPHOS anomalies [83].

### **Conclusion**

Lon knockdown induced a number of effects indicative of mitochondrial dysfunction in a context of oxidative stress. This mitochondrial dysfunction manifests in a particularly significant way through impaired energy metabolism. Moreover, the effects of Lon deficiency vary depending on the conditions showing more signs of mitochondrial alterations in galactose medium and much less when cells are grown under 3% O<sub>2</sub> that underscores the importance of the Lon protease in mitochondrial aerobic energy metabolisms and stress response as well as its privileged cooperation with such signaling pathways as the Nrf2-Keap1 pathway.

## References

- [1] A. Nickel, M. Kohlhaas, and C. Maack, “Mitochondrial reactive oxygen species production and elimination,” *J. Mol. Cell. Cardiol.*, vol. 73, pp. 26–33, 2014.
- [2] K. M. Holmström and T. Finkel, “Cellular mechanisms and physiological consequences of redox-dependent signalling,” *Nat. Rev. Mol. Cell Biol.*, vol. 15, no. 6, pp. 411–421, 2014.
- [3] A. Bayot, M. Gareil, A. Rogowska-Wrzesinska, P. Roepstorff, B. Friguet, and A. L. Bulteau, “Identification of novel oxidized protein substrates and physiological partners of the mitochondrial ATP-dependent Lon-like protease Pim1,” *J. Biol. Chem.*, vol. 285, no. 15, pp. 11445–11457, 2010.
- [4] M. P. Hamon, A. L. Bulteau, and B. Friguet, “Mitochondrial proteases and protein quality control in ageing and longevity,” *Ageing Res. Rev.*, vol. 23, no. PA, pp. 56–66, 2015.
- [5] T. Bender, C. Leidhold, T. Ruppert, S. Franken, and W. Voos, “The role of protein quality control in mitochondrial protein homeostasis under oxidative stress,” *Proteomics*, vol. 10, no. 7, pp. 1426–1443, Apr. 2010.
- [6] A. Bayot, M. Gareil, L. Chavatte, M.P. Hamon, C. L’Hermitte-Stead, F. Beaumatin, M. Priault, P. Rustin, A. Lombès, B. Friguet and A.L. Bulteau., “Effect of Lon protease knockdown on mitochondrial function in HeLa cells,” *Biochimie*, vol. 100, no. 1, pp. 38–47, May 2014.
- [7] A.L. Bulteau, L. I. Szweda, and B. Friguet, “Mitochondrial protein oxidation and degradation in response to oxidative stress and aging,” *Exp. Gerontol.*, vol. 41, no. 7, pp. 653–7, Jul. 2006.
- [8] D. A. Bota, J. K. Ngo, and K. J. A. Davies, “Downregulation of the human Lon protease impairs mitochondrial structure and function and causes cell death,” *Free Radic. Biol. Med.*, vol. 38, no. 5, pp. 665–77, Mar. 2005.
- [9] D. Bota, H. Van Remmen, and K. J. A. Davies, “Modulation of Lon protease activity and aconitase turnover during aging and oxidative stress,” *FEBS Lett.*, vol. 532, no. 1–2, pp. 103–6, Dec. 2002.
- [10] J. K. Ngo, L. C. D. Pomatto, D. A. Bota, A. L. Koop, and K. J. A. Davies, “Impairment of lon-induced protection against the accumulation of oxidized proteins in senescent Wi-38 fibroblasts,” *Journals Gerontol. - Ser. A Biol. Sci. Med. Sci.*, vol. 66 A, no. 11, pp. 1178–1185, 2011.
- [11] M. Pinti, L. Gibellini, M. Nasi, S. De Biasi, C. A. Bortolotti, A. Iannone, and A. Cossarizza., “Emerging role of Lon protease as a master regulator of mitochondrial functions,” *Biochim. Biophys. Acta - Bioenerg.*, vol. 1857, no. 8, pp. 1300–1306, 2016
- [12] W. J. H. Koopman, H.-J. Visch, J. A. M. Smeitink, and P. H. G. M. Willems, “Simultaneous quantitative measurement and automated analysis of mitochondrial morphology, mass, potential, and motility in living human skin fibroblasts,” *Cytom. Part A*, vol. 69A, no. 1, pp. 1–12, 2006.

- [13] E. K. Ahmed, A. Rogowska-Wrzesinska, P. Roepstorff, A.-L. Bulteau, and B. Friguet, "Protein modification and replicative senescence of WI-38 human embryonic fibroblasts.," *Aging Cell*, vol. 9, no. 2, pp. 252–72, Apr. 2010.
- [14] Y. Mallat, E. Tritsch, R. Ladouce, D.L. Winter, B.Friguet, Z. Li and M. Mericskay., "Proteome Modulation in H9c2 Cardiac Cells by microRNAs miR-378 and miR-378," *Mol. Cell. Proteomics*, vol. 13, no. 1, pp. 18–29, Jan. 2014.
- [15] A. Shevchenko, A. Loboda, and W. Ens, "Archived polyacrylamide gels as a resource for proteome characterization by mass spectrometry," *Electrophoresis*, vol. 22, no. 6, pp. 1194–1203, 2001.
- [16] J. K. Ngo, L. C. D. Pomatto, and K. J. A. Davies, "Upregulation of the mitochondrial Lon Protease allows adaptation to acute oxidative stress but dysregulation is associated with chronic stress, disease, and aging," *Redox Biol.*, vol. 1, no. 1, pp. 258–264, 2013.
- [17] J. V. Carletti, A. Correia-Branco, C. R. Silva, N. Andrade, L. O. P. Silva, and F. Martel, "The effect of oxidative stress induced by tert-butylhydroperoxide under distinct folic acid conditions: An in vitro study using cultured human trophoblast-derived cells," *Reprod. Toxicol.*, vol. 77, pp. 33–42, 2018.
- [18] I. Garcia, W. Innis-Whitehouse, A. Lopez, M. Keniry, and R. Gilkerson, "Oxidative insults disrupt OPA1-mediated mitochondrial dynamics in cultured mammalian cells," *Redox Rep.*, vol. 23, no. 1, pp. 160–167, 2018.
- [19] M. Fedorova, R. C. Bollineni, and R. Hoffmann, "Protein carbonylation as a major hallmark of oxidative damage: Update of analytical strategies," *Mass Spectrom. Rev.*, vol. 33, no. 2, pp. 79–97, 2014.
- [20] N. Chondrogianni, I. Petropoulos, S. Grimm, K. Georgila, B.Catalgol, B. Friguet, T.Grune and E.S. Gonos, "Molecular Aspects of Medicine Protein damage , repair and proteolysis," *Mol. Aspects Med.*, vol. 35, pp. 1–71, 2014.
- [21] R. Szklarczyk, M. Nooteboom, and H. D. Osiewacz, "Control of mitochondrial integrity in ageing and disease," *Philos. Trans. R. Soc. B Biol. Sci.*, vol. 369, no. 1646, 2014.
- [22] W. G. An, M. Kanekal, M. C. Simon, E. Maltepe, M. V. Blagosklonny, and L. M. Neckers, "Stabilization of wild-type p53 by hypoxia-inducible factor 1 $\alpha$ ," *Nature*, vol. 392, no. 6674, pp. 406–508, 1998.
- [23] M. A. Baraibar and B. Friguet, "Oxidative proteome modifications target specific cellular pathways during oxidative stress, cellular senescence and aging," *Exp. Gerontol.*, vol. 48, no. 7, pp. 620–625, 2013.
- [24] D. Zhang, J. Li, F. Wang, J. Hu, S. Wang, and Y. Sun, "2-Deoxy-D-glucose targeting of glucose metabolism in cancer cells as a potential therapy," *Cancer Lett.*, vol. 355, no. 2, pp. 176–183, 2014.
- [25] W. Duan and M. P. Mattson, "Dietary restriction and 2-deoxyglucose administration improve behavioral outcome and reduce degeneration of dopaminergic neurons in models of Parkinson's disease," *J. Neurosci. Res.*, vol. 57, no. 2, pp. 195–206, 1999.

- [26] N. Jelluma, “Glucose Withdrawal Induces Oxidative Stress followed by Apoptosis in Glioblastoma Cells but not in Normal Human Astrocytes,” *Mol. Cancer Res.*, vol. 4, no. 5, pp. 319–330, 2006.
- [27] T. J. Schulz, K. Zarse, A. Voigt, N. Urban, M. Birringer, and M. Ristow, “Glucose Restriction Extends *Caenorhabditis elegans* Life Span by Inducing Mitochondrial Respiration and Increasing Oxidative Stress,” *Cell Metab.*, vol. 6, no. 4, pp. 280–293, 2007.
- [28] M. H. A. Bakar, M. R. Sarmidi, C. K. Kai, H. Z. Huri, and H. Yaakob, “Amelioration of Mitochondrial Dysfunction-Induced Insulin Resistance in Differentiated 3T3-L1 Adipocytes via Inhibition of NF- $\kappa$ B Pathways,” *Int. J. Mol. Sci.*, vol. 15, no. 12, pp. 22227–22257, 2014.
- [29] L. A. Shchepina, O.Y. Pletjushkina, A.V. Avetisyan, L.E. Bakeeva<sup>1</sup>, E.K. Fetisova, D.S. Izyumov, V.B. Saprunova, M.Y. Vyssokikh, B.V. Chernyak and V.P. Skulachev, “Oligomycin, inhibitor of the F<sub>0</sub> part of H<sup>+</sup>-ATP-synthase, suppresses the TNF-induced apoptosis,” *Oncogene*, vol. 21, no. 53, pp. 8149–8157, 2002.
- [30] N. Zemirli, E. Morel, and D. Molino, “Mitochondrial dynamics in basal and stressful conditions,” *Int. J. Mol. Sci.*, vol. 19, no. 2, pp. 1–19, 2018.
- [31] C. Bo-Htay, S. Palee, N. Apaijai, S. C. Chattipakorn, and N. Chattipakorn, “Effects of d-galactose-induced ageing on the heart and its potential interventions,” *J. Cell. Mol. Med.*, vol. 22, no. 3, pp. 1392–1410, 2018.
- [32] D. M. Otte, T. Rasko, M. Wang, M. Dreiseidler, E. Drews, H. Schrage, A. Wojtalla, J. Hohfeld, E. Wanker and A. Zimmer, “Identification of the Mitochondrial MSRB2 as a Binding Partner of LG72,” *Cell. Mol. Neurobiol.*, vol. 34, no. 8, pp. 1123–1130, 2014.
- [33] M. Chatterjee, M. Andrulis, T. Stühmer, E. Müller, C. Hofmann, T. Steinbrunn, T. Heimberger, H. Schraud, S. Kressmann, H. Einsele and R.C. Bargou, “The PI3k/Akt signaling pathway regulates the expression of Hsp70, which critically contributes to Hsp90-chaperone function and tumor cell survival in multiple myeloma,” *Haematologica*, vol. 98, no. 7, pp. 1132–1141, 2013.
- [34] L. Giulino-Roth, H.J. van Besien, T. Dalton, J.E. Totonchy, A. Rodina, T. Taldone, A. Bolaender, H. Erdjument-Bromage, J. Sadek, A. Chadburn, M.J. Barth, F.S. Dela Cruz, A. Rainey, A.L. Kung, G. Chiosis and E. Cesarman, “Inhibition of Hsp90 Suppresses PI3K/AKT/mTOR Signaling and Has Antitumor Activity in Burkitt Lymphoma,” *Mol. Cancer Ther.*, vol. 16, no. 9, pp. 1779–1790, 2017.
- [35] L. O. Klotz, C. Sánchez-Ramos, I. Prieto-Arroyo, P. Urbánek, H. Steinbrenner, and M. Monsalve, “Redox regulation of FoxO transcription factors,” *Redox Biol.*, vol. 6, pp. 51–72, Dec. 2015.
- [36] A. T. Dinkova-Kostova and A. Y. Abramov, “The emerging role of Nrf2 in mitochondrial function,” *Free Radic. Biol. Med.*, vol. 88, no. Part B, pp. 179–188, 2015.

- [37] G. Tzivion, M. Dobson, and G. Ramakrishnan, “FoxO transcription factors; Regulation by AKT and 14-3-3 proteins,” *Biochim. Biophys. Acta - Mol. Cell Res.*, vol. 1813, no. 11, pp. 1938–1945, 2011.
- [38] K. Pennington, T. Chan, M. Torres, and J. Andersen, “The dynamic and stress-adaptive signaling hub of 14-3-3: emerging mechanisms of regulation and context-dependent protein–protein interactions,” *Oncogene*, vol. 37, no. 42, pp. 5587–5604, 2018.
- [39] G. M. DeNicola and I. S. Harris, “Making sense of reAKTive oxygen species,” *Cell Death Differ.*, vol. 23, no. 8, pp. 1269–1270, 2016.
- [40] A.B. Thrush, R. Zhang, W. Chen, E.L. Seifert, J.K. Quizi, R. McPherson, R. Dent and M.E. Harper, “Lower mitochondrial proton leak and decreased glutathione redox in primary muscle cells of obese diet-resistant versus diet-sensitive humans,” *J. Clin. Endocrinol. Metab.*, vol. 99, no. 11, pp. 4223–4230, 2014.
- [41] P. S. Brookes, “Mitochondrial H + leak and ROS generation: An odd couple,” *Free Radic. Biol. Med.*, vol. 38, no. 1, pp. 12–23, 2005.
- [42] A. S. Divakaruni and M. D. Brand, “The Regulation and Physiology of Mitochondrial Proton Leak,” *Physiology*, vol. 26, no. 3, pp. 192–205, 2011.
- [43] R. Rossignol, R. Gilkerson, R. Aggeler, K. Yamagata, S. J. Remington, and R. A. Capaldi, “Energy Substrate Modulates Mitochondrial Structure and Oxidative Capacity in Cancer Cells,” *Cancer Res.*, vol. 64, no. 3, pp. 985–993, 2004.
- [44] R. Domenis, E. Bisetto, D. Rossi, M. Comelli, and I. Mavelli, “Glucose-modulated mitochondria adaptation in tumor cells: A focus on ATP synthase and Inhibitor Factor 1,” *Int. J. Mol. Sci.*, vol. 13, no. 2, pp. 1933–1950, 2012.
- [45] A. M. Youle, R. J., & van der Blik, “Mitochondrial fission, fusion, and stress,” *Science (80-. )*, vol. 337, no. 6098, pp. 1062–1065, 2012.
- [46] O. Guillery, F. Malka, P. Frachon, D. Milea, M. Rojo, and A. Lombès, “Modulation of mitochondrial morphology by bioenergetics defects in primary human fibroblasts,” *Neuromuscul. Disord.*, vol. 18, no. 4, pp. 319–330, 2008.
- [47] P. M. Quirós, Y. Espanol, R. Acin-Perez, F. Rodriguez, C. Barcena, K. Watanabe, E. Calvo, M. Loureiro, M.S. Fernandez-Garcia, A. Fueyo, J. Vazquez, J.A. Enriquez and C. Lopez-Otin, “ATP-Dependent Lon Protease Controls Tumor Bioenergetics by Reprogramming Mitochondrial Activity,” *Cell Rep.*, vol. 8, no. 2, pp. 542–556, 2014.
- [48] T. MacVicar and T. Langer, “OPA1 processing in cell death and disease – the long and short of it,” *J. Cell Sci.*, vol. 129, no. 12, pp. 2297–2306, 2016.
- [49] J. Li, Q. Huang, X. Long, X. Guo, X. Sun, X. Jin, Z. Li, T. Ren, P. Yuan, X. Huang, H. Zhang and J. Xing, “Mitochondrial elongation-mediated glucose metabolism reprogramming is essential for tumour cell survival during energy stress,” *Oncogene*, vol. 36, no. 34, pp. 4901–4912, 2017.



- [50] W. J. H. Koopman, “Inhibition of complex I of the electron transport chain causes O<sub>2</sub><sup>•</sup>-mediated mitochondrial outgrowth,” *AJP Cell Physiol.*, vol. 288, no. 6, pp. C1440–C1450, 2005.
- [51] J. Chiche, M. Rouleau, P. Gounon, M. C. Brahimi-Horn, J. Pouyssegur, and N. M. Mazure, “Hypoxic enlarged mitochondria protect cancer cells from apoptotic stimuli,” *J. Cell. Physiol.*, vol. 222, no. 3, pp. 648–657, 2010.
- [52] T. Shutt, M. Geoffrion, R. Milne, and H. M. McBride, “The intracellular redox state is a core determinant of mitochondrial fusion,” *EMBO Rep.*, vol. 13, no. 10, pp. 909–915, 2012.
- [53] R. Fukuda, H. Zhang, J. Kim, L. Shimoda, C. V Dang, and G. L. Semenza, “HIF-1 regulates cytochrome oxidase subunits to optimize efficiency of respiration in hypoxic cells,” *Cell*, vol. 129, no. 1, pp. 111–22, Apr. 2007.
- [54] O. Hori, F. Ichinoda, T. Tamatani, A. Yamaguchi, N. Sato, K. Ozawa, Y. Kitao, M. Miyazaki, H. P. Harding, D. Ron, M. Tohyama, D. M. Stern, and S. Ogawa, “Transmission of cell stress from endoplasmic reticulum to mitochondria: Enhanced expression of Lon protease,” *J. Cell Biol.*, vol. 157, no. 7, pp. 1151–1160, 2002.
- [55] S. Venkatesh, J. Lee, K. Singh, I. Lee, and C. K. Suzuki, “Multitasking in the mitochondrion by the ATP-dependent Lon protease,” *Biochim. Biophys. Acta - Mol. Cell Res.*, vol. 1823, no. 1, pp. 56–66, 2012.
- [56] R. Sabouny, E. Fraunberger, M. Geoffrion, A. C. Ng, S. D. Baird, R.A. Screatton, R. Milne, H. M. McBride, and T. E. Schutt, “The Keap1-Nrf2 Stress Response Pathway Promotes Mitochondrial Hyperfusion Through Degradation of the Mitochondrial Fission Protein Drp1,” *Antioxidants Redox Signal.*, vol. 27, no. 18, pp. 1447–1459, 2017.
- [57] Y. S. Yoon, H. O. Byun, H. Cho, B. K. Kim, and G. Yoon, “Complex II Defect via Down-regulation of Iron-Sulfur Subunit Induces Mitochondrial Dysfunction and Cell Cycle Delay in Iron Chelation-induced Senescence-associated Growth Arrest,” *J. Biol. Chem.*, vol. 278, no. 51, pp. 51577–51586, 2003.
- [58] K. Fujisawa, T. Takami, S. Okada, K. Hara, T. Matsumoto, N. Yamamoto, T. Yamasaki, and I. Sakaida, “Analysis of Metabolomic Changes in Mesenchymal Stem Cells on Treatment with Desferrioxamine as a Hypoxia Mimetic Compared with Hypoxic Conditions,” *Stem Cells*, vol. 36, no. 8, pp. 1226–1236, 2018.
- [59] Y. S. Lee and R. D. Wurster, “Deferoxamine-induced cytotoxicity in human neuronal cell lines: protection by free radical scavengers,” *Toxicol. Lett.*, vol. 78, no. 1, pp. 67–71, 1995.
- [60] G. Sgarbi, G. Gorini, A. Costanzini, S. Barbato, G. Solaini, and A. Baracca, “Hypoxia decreases ROS level in human fibroblasts,” *Int. J. Biochem. Cell Biol.*, vol. 88, no. December 2016, pp. 133–144, 2017.
- [61] J. Li, C.-X. Zhang, Y.-M. Liu, K.-L. Chen, and G. Chen, “A comparative study of anti-aging properties and mechanism: resveratrol and caloric restriction,” *Oncotarget*, vol. 8, no. 39, pp. 65717–65729, 2017.

- [62] D. Delwing-de Lima, M. Fröhlich, L. Dalmedico, J.G.M. Aurélio, D. Delwing-Dal Magro, E.M. Pereira and A.T.S. Wyse, “Galactose alters markers of oxidative stress and acetylcholinesterase activity in the cerebrum of rats: protective role of antioxidants,” *Metab. Brain Dis.*, vol. 32, no. 2, pp. 359–368, 2017.
- [63] L. R. Saunders and E. Verdin, “Sirtuins: Critical regulators at the crossroads between cancer and aging,” *Oncogene*, vol. 26, no. 37, pp. 5489–5504, 2007.
- [64] F. Dong, S. Wang, Y. Wang, X. Yang, J. Jiang, D. Wu, X. Qu, H. Fan and R. Yao, “Quercetin ameliorates learning and memory via the Nrf2-ARE signaling pathway in D-galactose-induced neurotoxicity in mice,” *Biochem. Biophys. Res. Commun.*, vol. 491, no. 3, pp. 636–641, 2017.
- [65] M. Pinti *et al.*, “Functional characterization of the promoter of the human Lon protease gene,” *Mitochondrion*, vol. 11, no. 1, pp. 200–206, 2011.
- [66] S. Krick *et al.*, “Mpv17l protects against mitochondrial oxidative stress and apoptosis by activation of Omi / HtrA2 protease,” 2008.
- [67] T. B. Zhou, Y. H. Qin, F. Y. Lei, W. F. Huang, and G. P. C. Drummen, “Prohibitin is associated with antioxidative protection in hypoxia/reoxygenation-induced renal tubular epithelial cell injury,” *Sci. Rep.*, vol. 3, pp. 1–8, 2013.
- [68] T. S. Blacker and M. R. Duchon, “Investigating mitochondrial redox state using NADH and NADPH autofluorescence,” *Free Radic. Biol. Med.*, vol. 100, pp. 53–65, 2016.
- [69] M. Gueugneau *et al.*, “Proteomics of muscle chronological ageing in post-menopausal women,” *BMC Genomics*, vol. 15, pp. 1–24, 2015.
- [70] Mullarky E.; Cantley L., “Diverting Glycolysis to Combat Oxidative Stress,” *Innov. Med. Basic Res. Dev.*, 2015.
- [71] F. Reinecke, J. A. M. Smeitink, and F. H. van der Westhuizen, “OXPHOS gene expression and control in mitochondrial disorders,” *Biochim. Biophys. Acta - Mol. Basis Dis.*, vol. 1792, no. 12, pp. 1113–1121, 2009.
- [72] H. J. Wright *et al.*, “CDCP1 drives triple-negative breast cancer metastasis through reduction of lipid-droplet abundance and stimulation of fatty acid oxidation,” *Proc. Natl. Acad. Sci.*, vol. 114, no. 32, pp. E6556–E6565, 2017.
- [73] F. Castro-Chavez *et al.*, “Coordinated Upregulation of Oxidative Pathways and Downregulation of Lipid Biosynthesis Underlie Obesity Resistance in Perilipin Knockout Mice: A Microarray Gene Expression Profile,” *Diabetes*, vol. 52, no. 11, pp. 2666–2674, 2003.
- [74] J. Yao, R. W. Irwin, L. Zhao, J. Nilsen, R. T. Hamilton, and R. D. Brinton, “Mitochondrial bioenergetic deficit precedes Alzheimer’s pathology in female mouse model of Alzheimer’s disease,” *Proc. Natl. Acad. Sci. U. S. A.*, vol. 106, no. 34, pp. 14670–14675, 2009.
- [75] C. Desler, T. L. Hansen, J. B. Frederiksen, M. L. Marcker, K. K. Singh, and L. Juel Rasmussen, “Is there a link between mitochondrial reserve respiratory capacity and aging?,” *J. Aging Res.*, vol. 2012, 2012.

- [76] Z.-P. Lv, Y.-Z. Peng, B.-B. Zhang, H. Fan, D. Liu, and Y.-M. Guo, "Glucose and lipid metabolism disorders in the chickens with dexamethasone-induced oxidative stress," *J. Anim. Physiol. Anim. Nutr. (Berl.)*, vol. 7, no. August, pp. 1–12, 2017.
- [77] M. F. Beal, "Aging, energy, and oxidative stress in neurodegenerative diseases," *Ann. Neurol.*, vol. 38, no. 3, pp. 357–366, 1995.
- [78] J. T. Legault *et al.*, "A Metabolic Signature of Mitochondrial Dysfunction Revealed through a Monogenic Form of Leigh Syndrome," vol. 13, no. 5, pp. 981–989, 2015.
- [79] R. K. J. Olsen, N. Cornelius, and N. Gregersen, "Redox signalling and mitochondrial stress responses; lessons from inborn errors of metabolism," *J. Inherit. Metab. Dis.*, vol. 38, no. 4, pp. 703–719, 2015.
- [80] A. Kuehne *et al.*, "Acute Activation of Oxidative Pentose Phosphate Pathway as First-Line Response to Oxidative Stress in Human Skin Cells," *Mol. Cell*, vol. 59, no. 3, pp. 359–371, 2015.
- [81] J. D. Arroyo *et al.*, "A Genome-wide CRISPR Death Screen Identifies Genes Essential for Oxidative Phosphorylation," *Cell Metab.*, vol. 24, no. 6, pp. 875–885, 2016.
- [82] B. H. Robinson, R. Petrova-Benedict, J. R. Buncic, and D. C. Wallace, "Nonviability of cells with oxidative defects in galactose medium: A screening test for affected patient fibroblasts," *Biochem. Med. Metab. Biol.*, vol. 48, no. 2, pp. 122–126, 1992.
- [83] K. Birsoy, T. Wang, W. W. Chen, E. Freinkman, M. Abu-Remaileh, and D. M. Sabatini, "An Essential Role of the Mitochondrial Electron Transport Chain in Cell Proliferation Is to Enable Aspartate Synthesis," *Cell*, vol. 162, no. 3, pp. 540–551, 2015.

## Legend figures

**Fig 1. Quantitative analysis of mitochondrial morphology, detection of oxidatively modified proteins and mitochondrial ROS production.** **A)** Average value of aspect ratio (AR) factor. After 10 days of induction with doxycycline, under different conditions (glucose, galactose, 2-DG, oligomycin, tBH, 3% oxygen, DFO), control (Dox-) or Lon-depleted (Dox+) cells were plated at subconfluence. After fixation in 4% paraformaldehyde and 0.1% glutaraldehyde, mitochondrial compartment was visualized using polyclonal antibodies against cytochrome c oxidase subunit 2. After acquisition and binarization of fluorescent images, mitochondrial network morphology was measured using the calculation of the Aspect Ratio (AR). Data represent the mean  $\pm$  SEM (n=30); Mann-Whitney test: \*p<0.05, \*\*\*p<0.001. **B)** AR factor ratio (Dox+/Dox-), n=30. **C)** Carbonylated proteins levels of cell extracts. Total cell extracts were prepared from control (Dox-) or Lon-depleted (Dox+) cells after 10 days of induction with doxycycline, under different conditions (glucose, galactose, 2-DG, oligomycin, tBH, 3% oxygen, DFO). Data represent the mean  $\pm$  SEM (n=3 to 10); Student t test: \*p<0.05, \*\*p<0.01. **D)** Ratios Dox+/Dox- of carbonylated proteins levels of cell extracts, n=3 to 5, Mann-Whitney test: \*\*p<0.01. **E)** Superoxide production measured using MitoSox fluorescent intensity levels under glucose or galactose conditions. Data are normalized to the glucose Dox- condition and represent the mean  $\pm$  SEM (n=3 to 6); Student t test: \*\*p<0.01. **F)** Carbonylated proteins levels of mitochondrial fractions extracts. Mitochondrial extracts were prepared from control (Dox-) or Lon-depleted (Dox+) cells after 10 days of induction with doxycycline under glucose or galactose conditions. Data are normalized to the glucose Dox- condition and represent the mean  $\pm$  SEM (n=3 to 4); Student t test: \*\*p<0.01.

**Fig 2. Mitochondrial protein quality control response.** Western blot analysis of mitochondrial proteins involved in protein quality control in whole cells homogenate of control (Dox-) or Lon-depleted (Dox+) cells after 10 days of induction with doxycycline, under glucose or galactose condition. Representative Western blots of the amount of **A)** ClpP, Mann-Whitney test: \*p<0.05, \*\*p<0.01; **B)** MsrB2, Student t test: \*\*p<0.01. Data are normalized to glucose Dox- condition and represent the mean  $\pm$  SEM (n=5 to 6).

**Fig 3. 2D DIGE and DeCyder analysis of proteomes of mitochondrial fractions.** **A)** Representative 2D DIGE gel images of proteins of mitochondrial fractions of HeLa cells cultured in glucose medium with or without Lon depletion. After being labeled with CyDyes, proteins were electrofocused, separated on gradient acrylamide SDS-PAGE and scanned. The combined protein profile of internal standard and samples named Glucose Dox+1 and Glucose Dox-5 shows green spots (proteins up-expressed in the Glucose Dox+1 sample), red spots (proteins up-expressed in the Glucose Dox-5 sample) and white spots (unchanged expression). **B)** Principal component analysis (PCA) showing the distribution of Cy3- and Cy5-labeled DIGE spots of interest (fold change  $\geq$ 1.3; p value  $\leq$  0,05) of 14 samples separated on the basis of the differentially expressed protein under glucose or galactose conditions. **C)** Using UniProt data, classification based on biological functions of proteins identified by mass spectrometry with significant expression modification in Lon-depleted (Dox+) cells compared to control (Dox-) cells.

**Fig 4. Cellular pathways analysis of proteins reported to be modified by Lon down-regulation through the use of Ingenuity Pathways Analysis (Ingenuity Systems, <http://www.ingenuity.com/>).** Analysis with Ingenuity Pathway of protein involved in quality control and stress response under **A)** glucose or **B)** galactose condition. Proteins in red and green correspond respectively to some of the proteins identified as overexpressed or under-expressed when Lon is down-regulated. Proteins in grey correspond to some of the proteins modified but not significantly when Lon is down-regulated. White open nodes indicate proteins not identified in this analysis, but associated with the regulation of some of the proteins identified. A line denotes binding of proteins, whereas a line with an arrow denotes “acts on.” A dotted line denotes an indirect interaction. Areas 1 to 4 point out groups of proteins covered in the results and the discussion.

**Fig 5. Oxidative stress response.** Western blot analysis of transcription factors involved in oxidative stress response in whole cells homogenate of control (Dox-) or Lon-depleted (Dox+) cells after 10 days of induction with doxycycline, under glucose or galactose condition. Representative Western blots of the amount of **A)** FoxO3, Student t test: \*\* $p < 0.01$ ; **B)** Nrf2, Student t test: \*\* $p < 0.01$ . Data are normalized to glucose Dox- condition and represent the mean  $\pm$  SEM (n=4 to 5).

**Fig 6. Differentially expressed proteins reported to act in energy metabolism upon Lon depletion.** Differentially expressed proteins involved in **A)** glycolysis and **B)** oxidative phosphorylation. Proteins in red and green correspond respectively to some of the proteins identified as overexpressed or under-expressed when Lon is down-regulated. Proteins in grey correspond to some of the proteins modified but not significantly when Lon is down-regulated. Abbreviations: HK, hexokinase; PGI, phosphoglucose isomerase; PFK, phosphofructo-kinase-1; ALDO, aldolase; TPI, triose phosphate isomerase; GAPDH, glyceraldehyde 3-phosphate dehydrogenase; PGK, phosphoglycerate kinase; PGM, phosphoglycero-mutase; ENO, enolase; PK, pyruvate kinase.

**Fig 7. ECAR and OCR in glucose or galactose medium with or without Lon depletion.** **A)** Extracellular acidification rate (ECAR) and **B)** oxygen consumption rate (OCR) were measured in a Seahorse XF24 analyzer. Each data-point represents mean  $\pm$  SEM, n=3. Cells were seeded at a density of 80,000. Glucose 10mM, galactose 10 $\mu$ M, oligomycin 1 $\mu$ M, 2-Deoxy-D-glucose 100mM, FCCP 1 $\mu$ M and rotenone 10 $\mu$ M were injected at the times indicated by the arrows. **C)** Basal OCR versus basal ECAR calculated from the data points 4,5,6 after glucose or galactose injection. **D)** The basal respiration OCR was calculated using the difference between the mean OCR of time points 1 to 3 (baseline) and the mean OCR of time points 10 to 12 (rotenone treatment). **E)** The ATP linked respiration OCR was calculated using the difference between the mean OCR of time points 1 to 3 (baseline) and the mean OCR of time points 4 to 6 (oligomycin treatment). **F)** The maximal respiratory capacity respiration OCR was calculated using the difference between the mean OCR of time points 7 to 9 (FCCP treatment) and the mean OCR of time points 10 to 12 (rotenone treatment). **G)** The reserve respiratory capacity OCR was calculated using the difference between the mean OCR of time points 7 to 9 (FCCP treatment) and the mean OCR of time points 1 to 3 (baseline). **H)** The proton leak respiration OCR was calculated using the difference between the mean OCR of time points 4 to 6 (oligomycin treatment) and the mean OCR of time points 10 to 12 (rotenone treatment). **I)** The glycolysis ECAR was calculated using the difference between the mean ECAR of time points

4 to 6 (glucose or galactose treatment) and the mean ECAR of time points 10 to 12 (2-DG treatment). **J**) The glycolytic capacity ECAR was calculated using the difference between the mean ECAR of time points 7 to 9 (oligomycin treatment) and the mean ECAR of time points 10 to 12 (2-DG treatment). **K**) The glycolytic reserve ECAR was calculated using the difference between the mean OCR of time points 7 to 9 (oligomycin treatment) and the mean ECAR of time points 4 to 6 (glucose or galactose treatment). One-way ANOVA test or Kruskal-Wallis test: \* $p < 0.05$ , \*\* $p < 0.01$ .

**Fig 8. Cell proliferation and ATP production.** **A**) Detection of proliferation in control (Dox-) or Lon-depleted (Dox+) cells after 10 days of induction with doxycycline, under glucose or galactose condition. Cells were treated with 10  $\mu$ M EdU for 4 hr, then detected an Alexa Fluor™ 488 azide (green). Cells were counterstained with DAPI (blue). **B**) Quantification of EdU-positive cells. Data represent the mean  $\pm$  SEM (n=3 to 5); Student t test: \* $p < 0.05$ . **C**) CellTiter-Glo assay measuring cellular ATP levels of control (Dox-) or Lon-depleted (Dox+) cells after 10 days of induction with doxycycline, under glucose or galactose condition. Data are normalized to the glucose Dox- condition and represent the mean  $\pm$  SEM (n=3); Student t test: \* $p < 0.05$ , \*\* $p < 0.01$ .

### Supplementary data

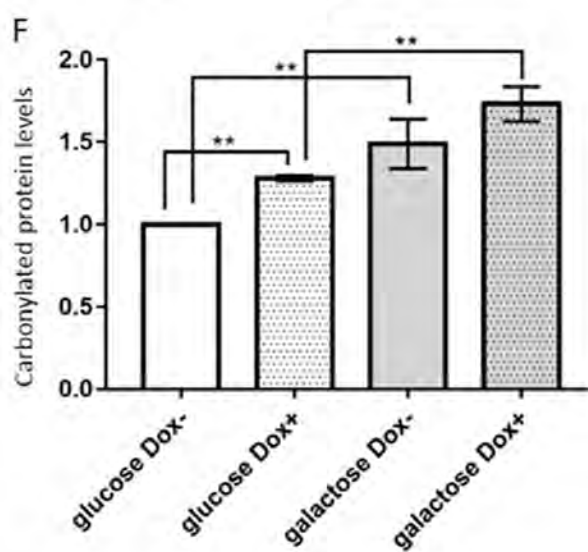
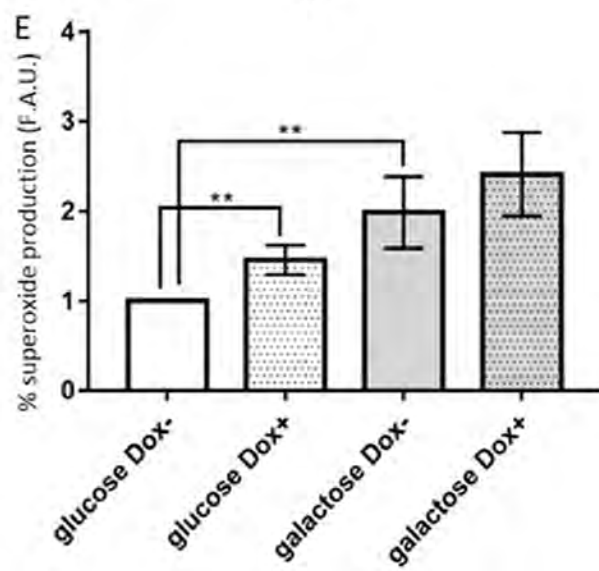
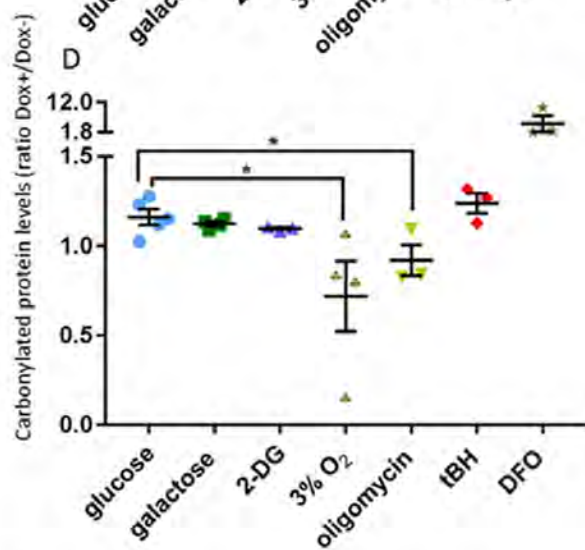
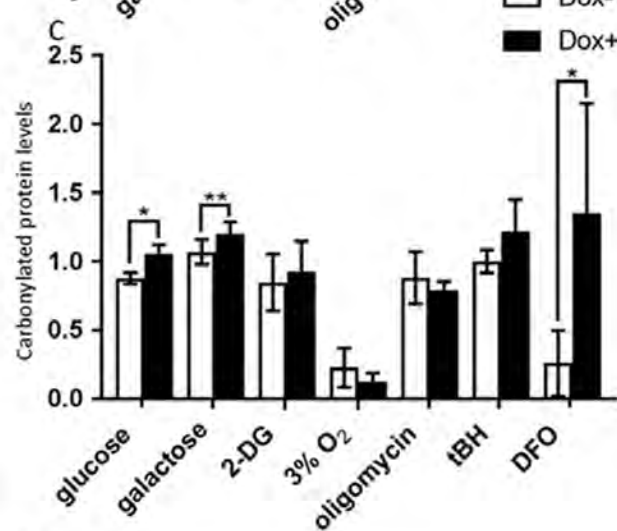
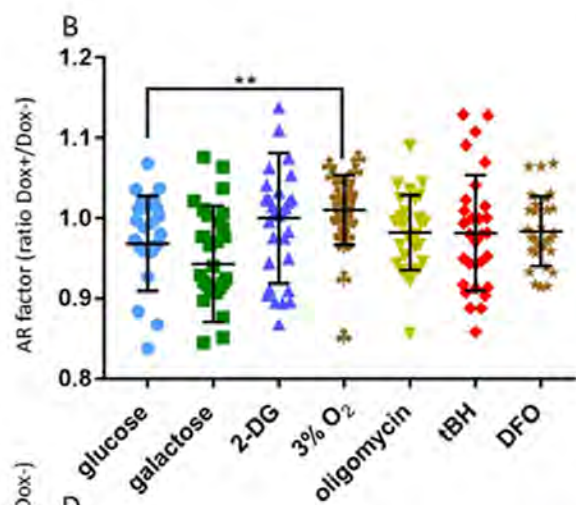
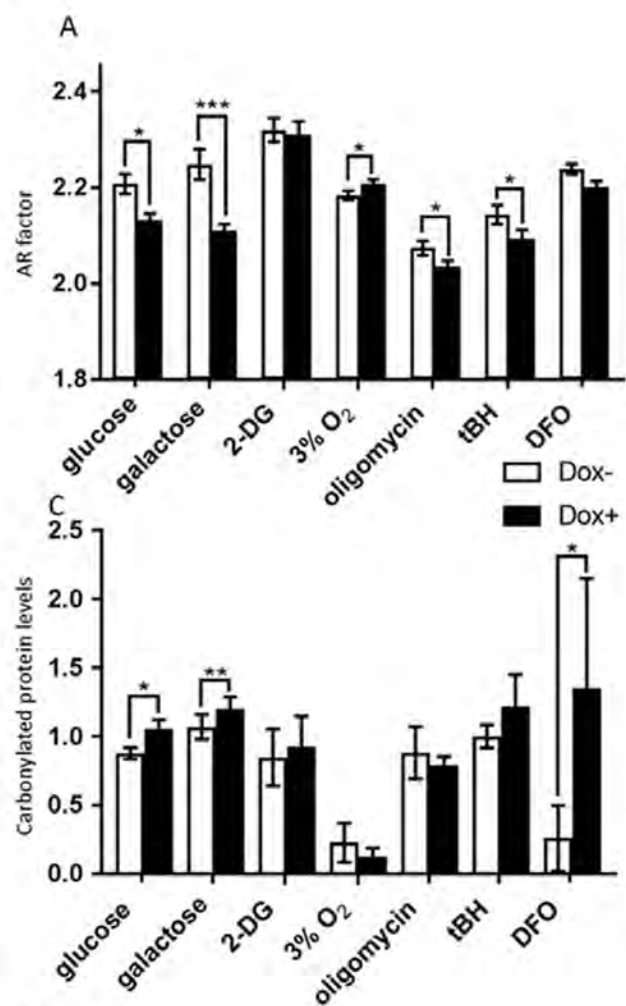
**Table 1. Protein overexpressed in glucose condition upon Lon depletion.** Protein identification of 2D DIGE-identified differentially expressed spots in mitochondrial fractions of HeLa cells cultured in glucose medium with or without Lon depletion. Spots of interest (fold change  $\geq 1.2$ ; ANOVA test  $p \leq 5\%$ , n = 4) were identified by mass spectrometry as described in Materials and methods. Proteins expressed in whole or in part in mitochondria are mentioned in red.

**Table 2. Protein down-expressed in glucose condition upon Lon depletion.** Protein identification of 2D DIGE-identified differentially expressed spots in mitochondrial fractions of HeLa cells cultured in glucose medium with or without Lon depletion. Spots of interest (fold change  $\geq 1.2$ ; ANOVA test  $p \leq 5\%$ , n = 4) were identified by mass spectrometry as described in Materials and methods. Proteins expressed in whole or in part in mitochondria are mentioned in red.

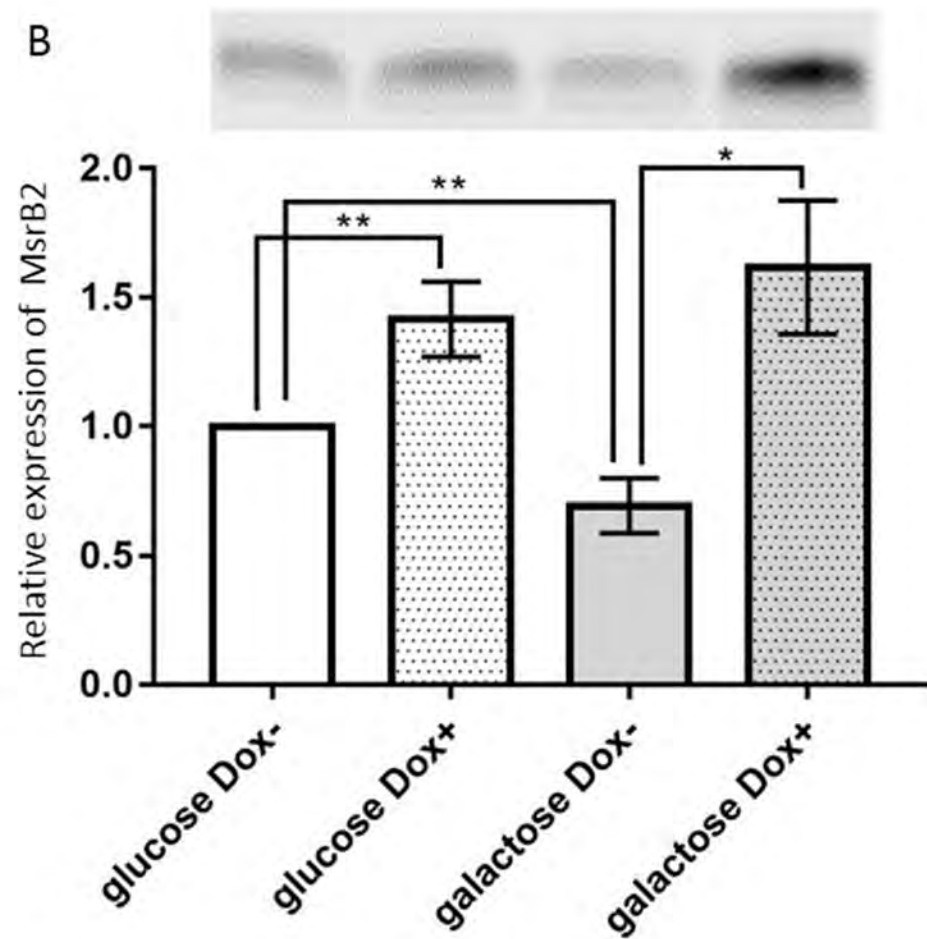
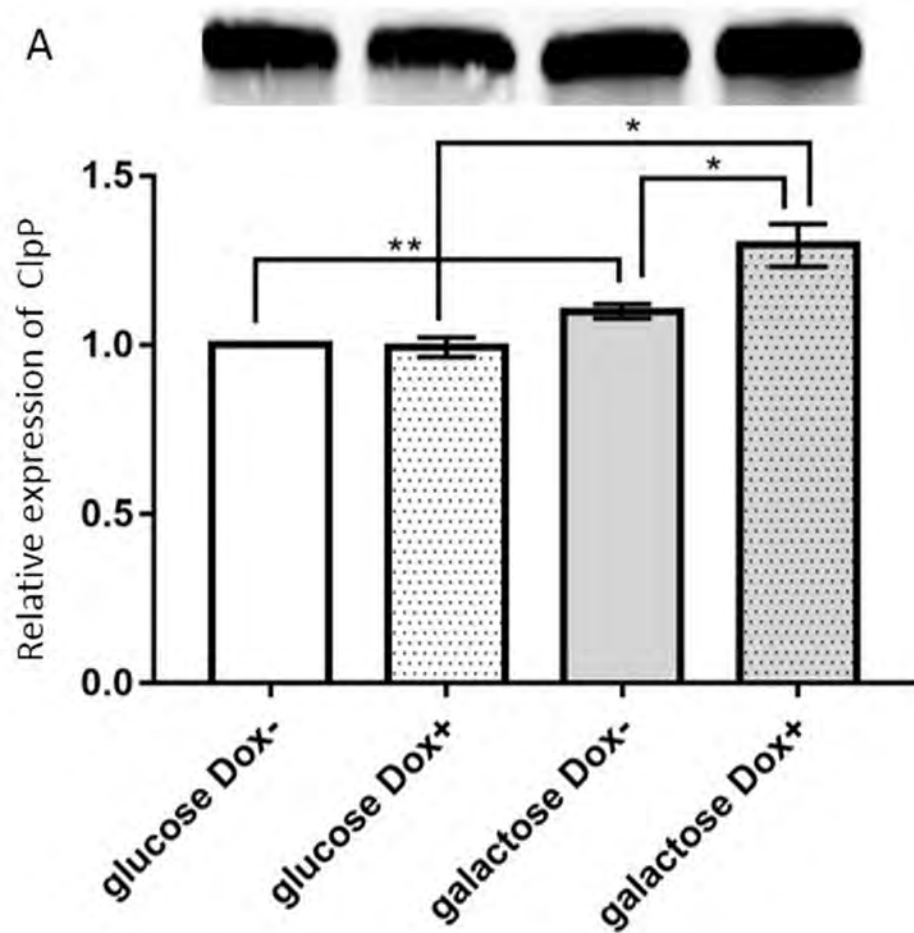
**Table 3. Protein overexpressed in galactose condition upon Lon depletion.** Protein identification of 2D DIGE-identified differentially expressed spots in mitochondrial fractions of HeLa cells cultured in galactose medium with or without Lon depletion. Spots of interest (fold change  $\geq 1.2$ ; ANOVA test  $p \leq 5\%$ , n = 4) were identified by mass spectrometry as described in Materials and methods. Proteins expressed in whole or in part in mitochondria are mentioned in red.

**Table 4. Protein down-expressed in galactose condition upon Lon depletion.** Protein identification of 2D DIGE-identified differentially expressed spots in mitochondrial fractions of HeLa cells cultured in galactose medium with or without Lon depletion. Spots of interest (fold change  $\geq 1.2$ ; ANOVA test  $p \leq 5\%$ , n = 4) were identified by mass spectrometry as

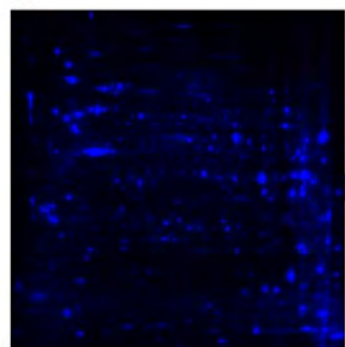
described in Materials and methods. Proteins expressed in whole or in part in mitochondria are mentioned in red.







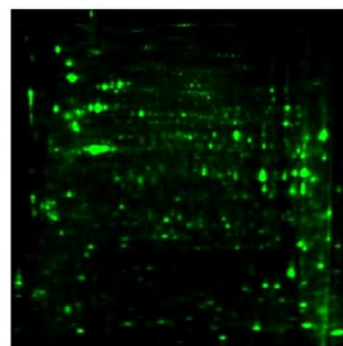
A



Cy 2



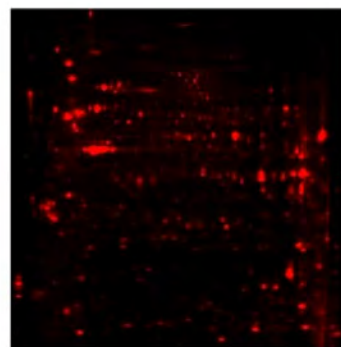
Internal  
standard



Cy 3



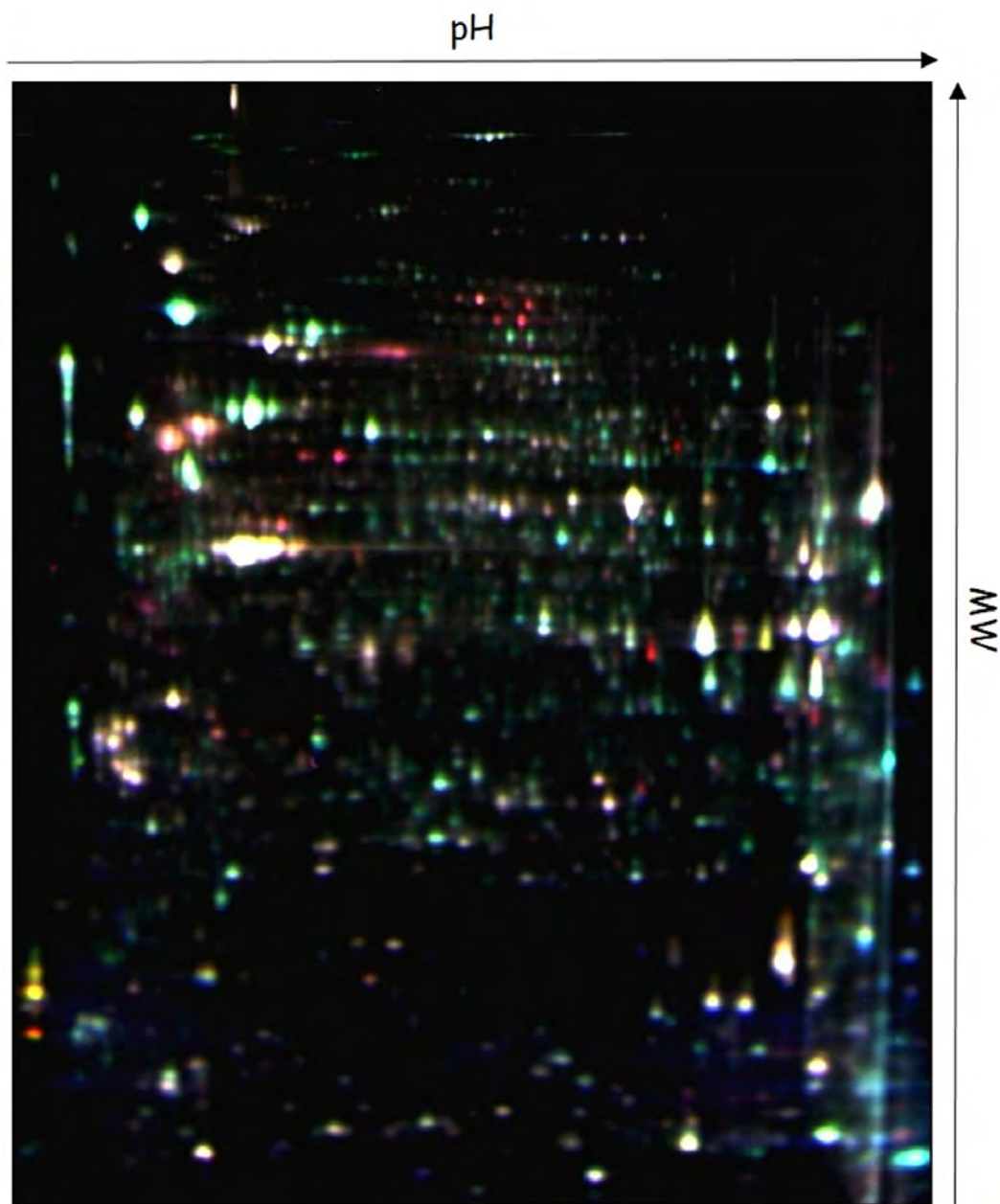
Glucose  
Dox+1



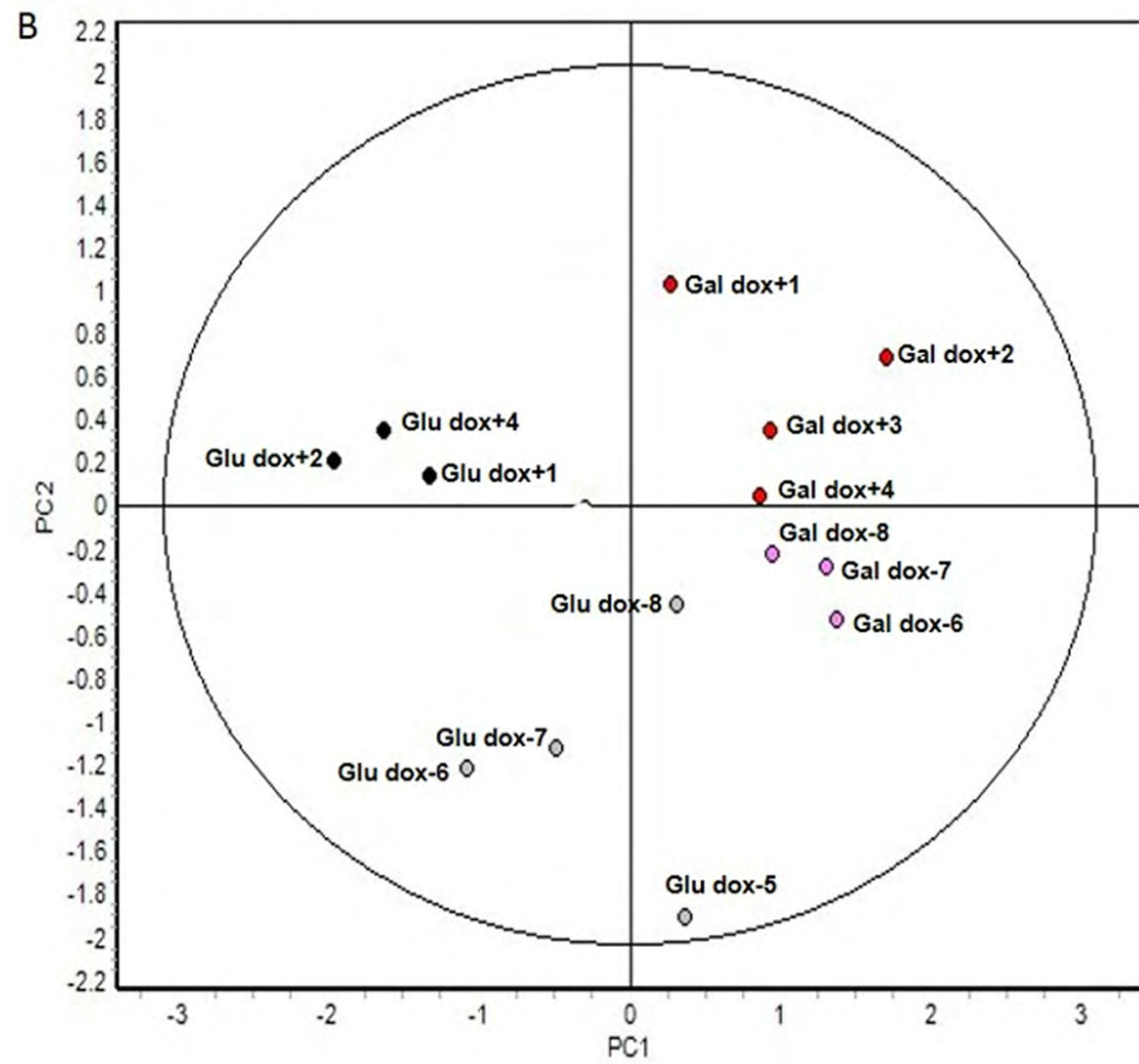
Cy 5



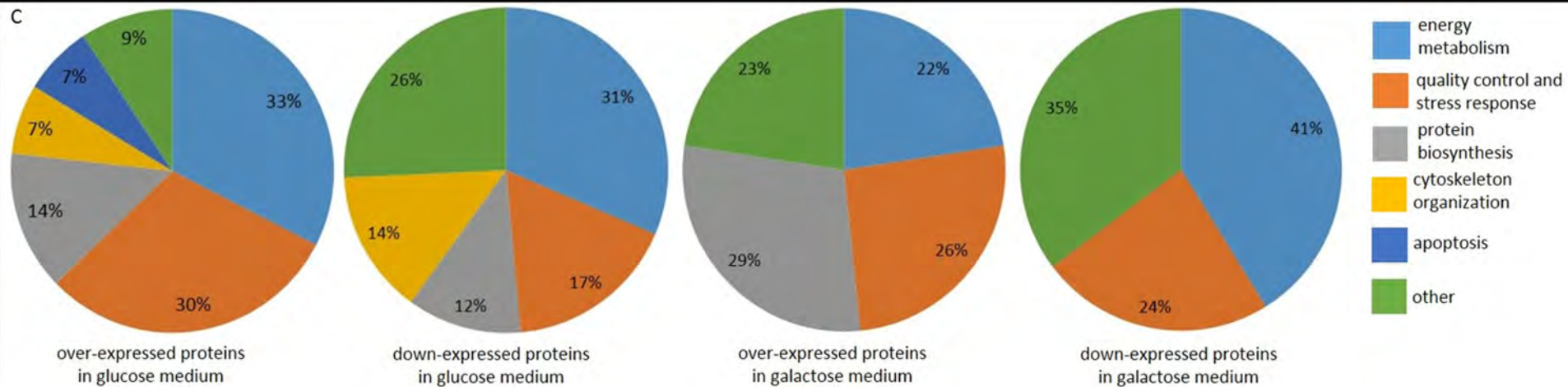
Glucose  
Dox-5



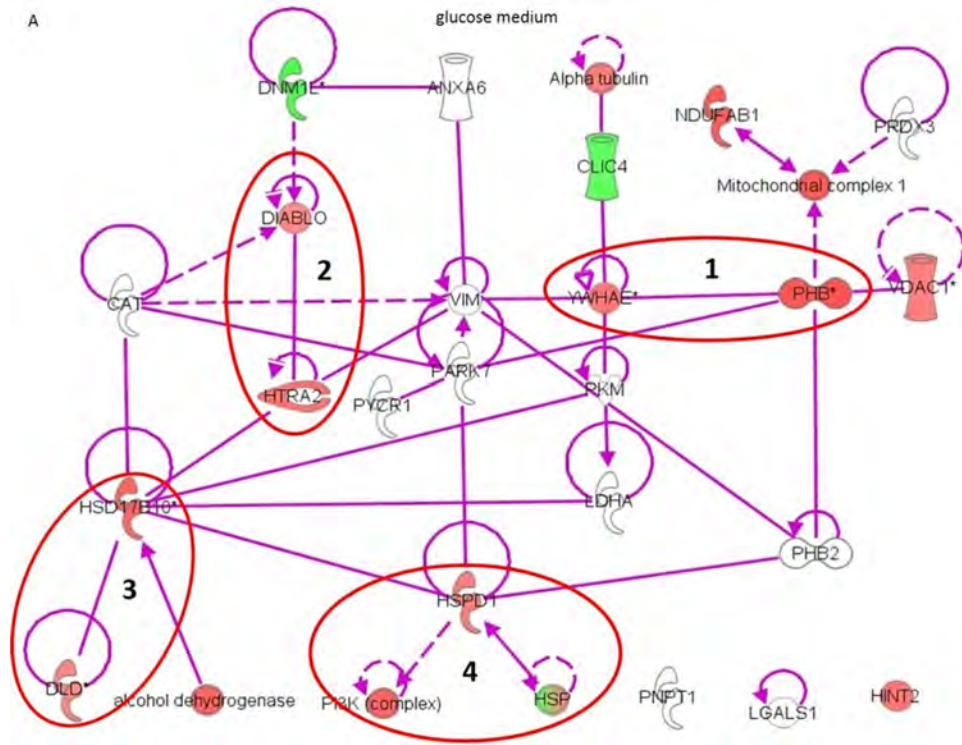
## Spot Maps (Score Plot)



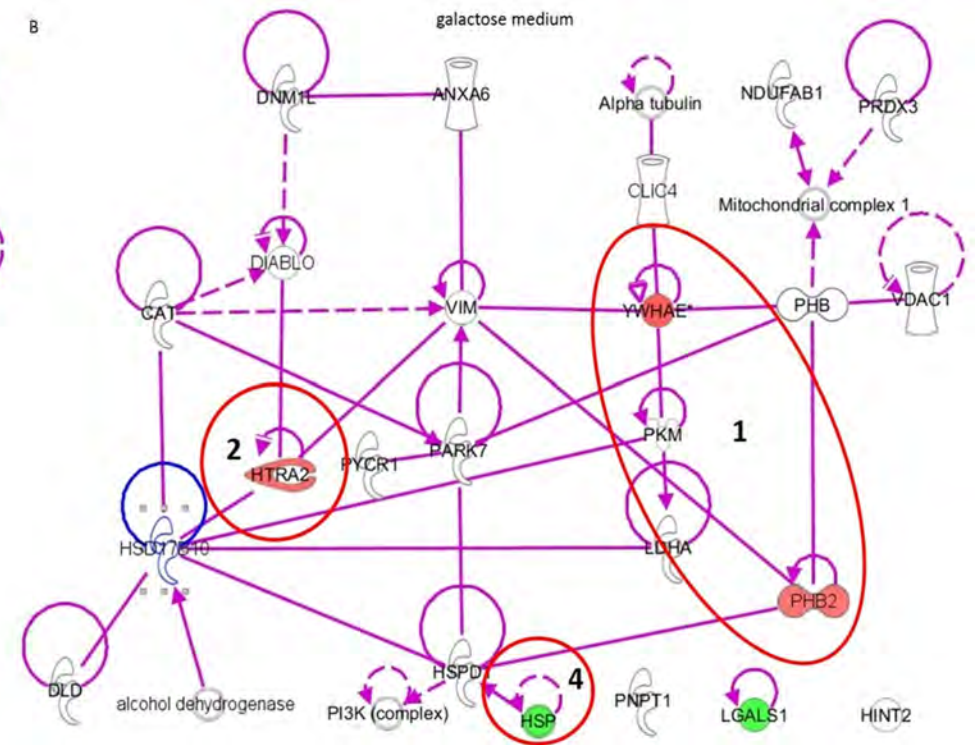
C

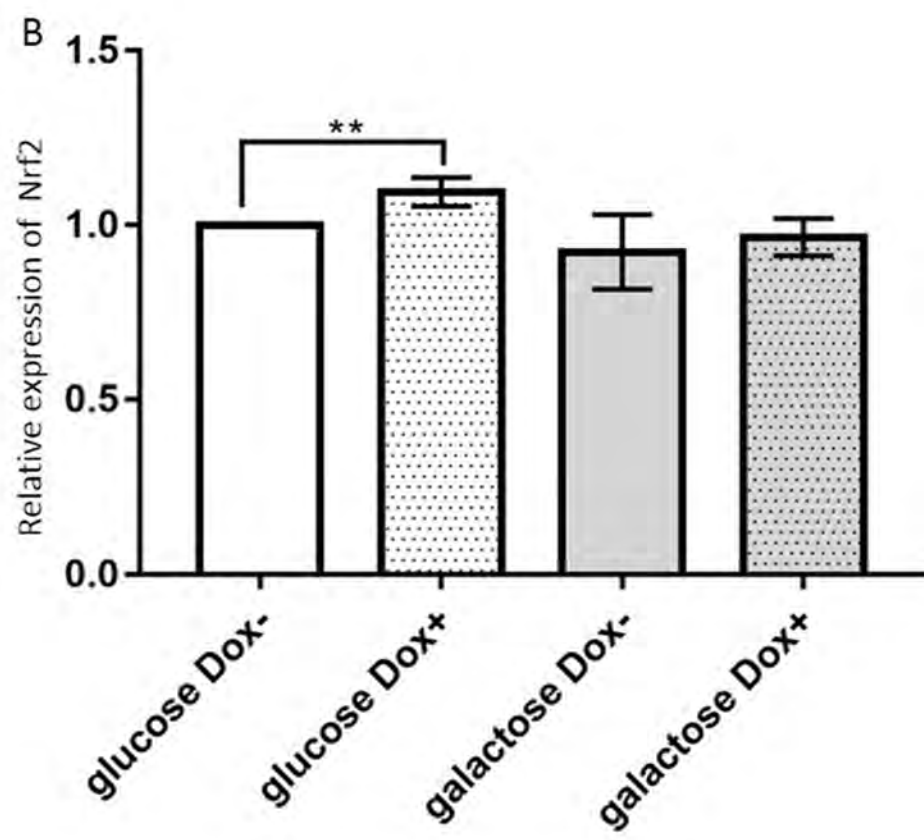
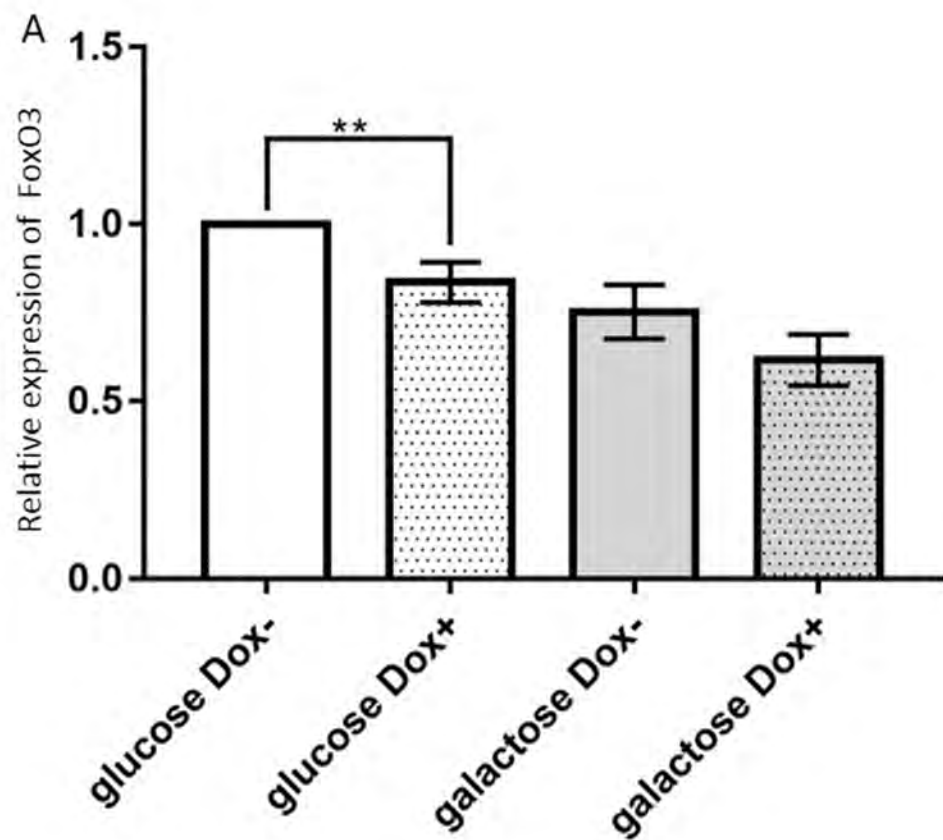


A

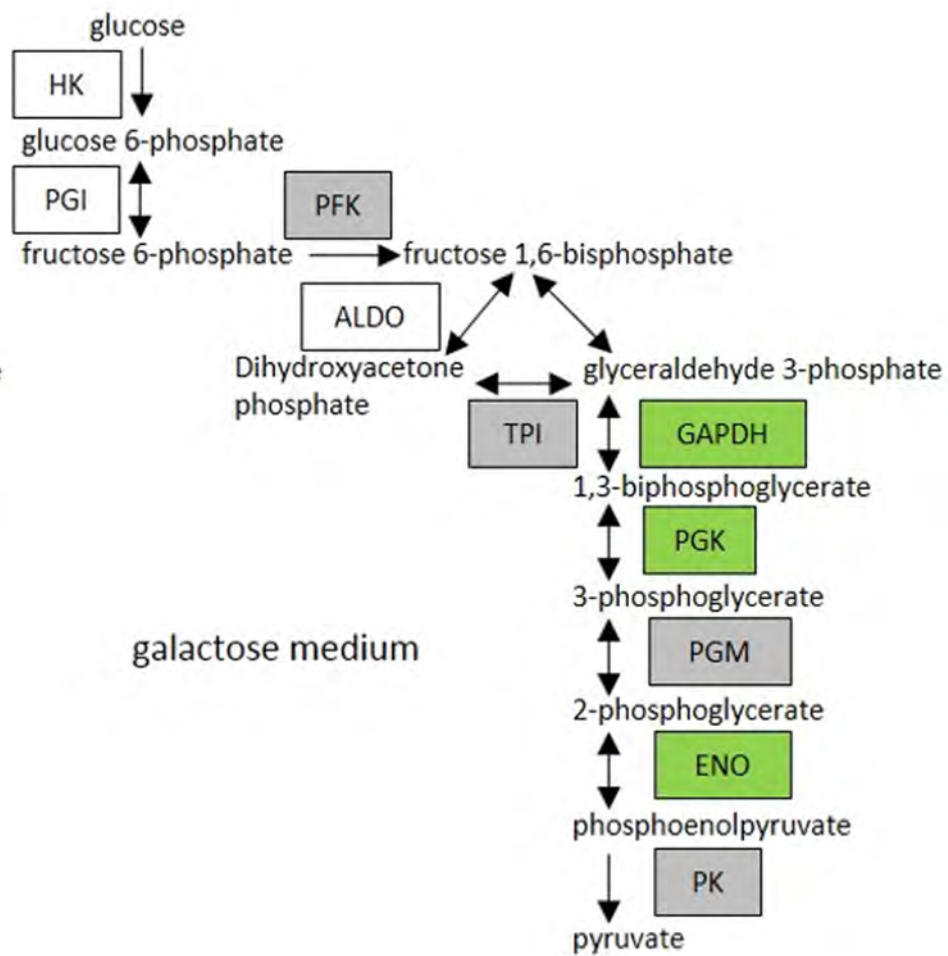
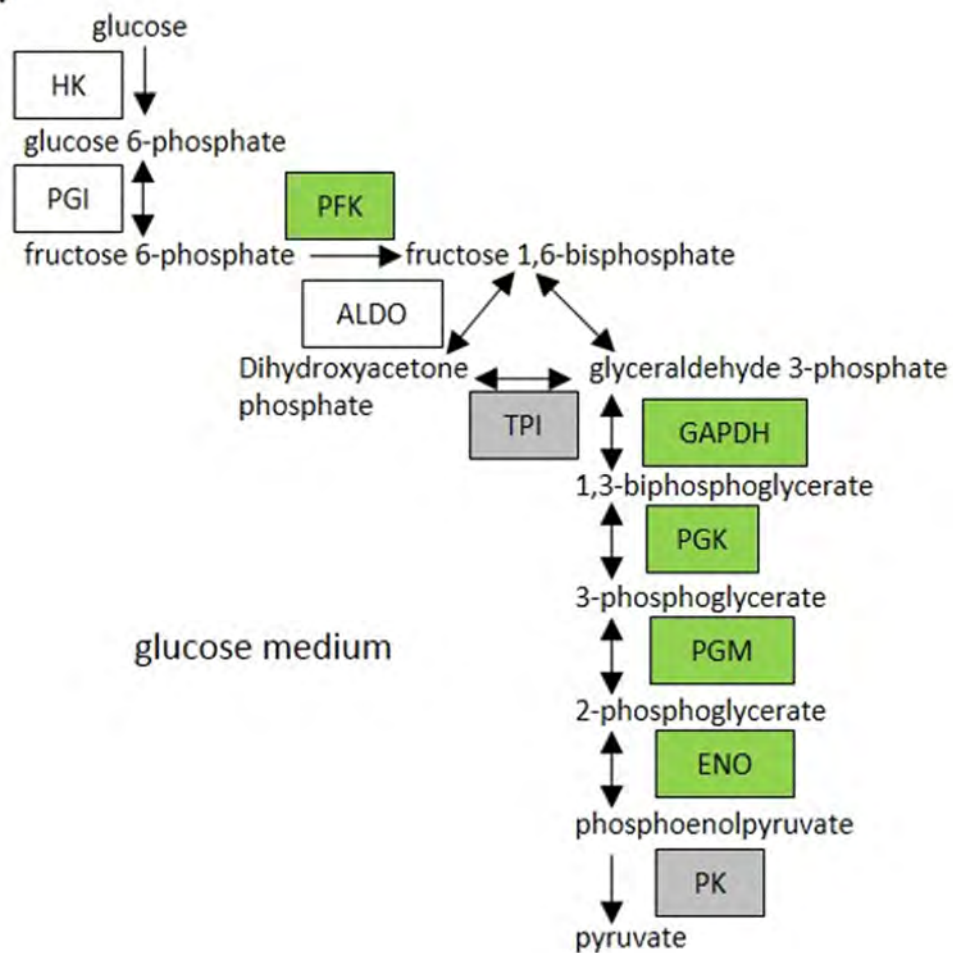


B



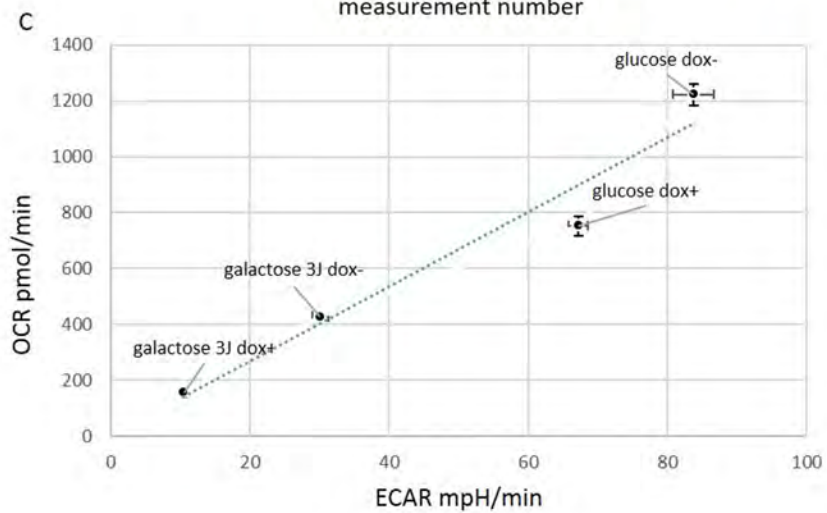
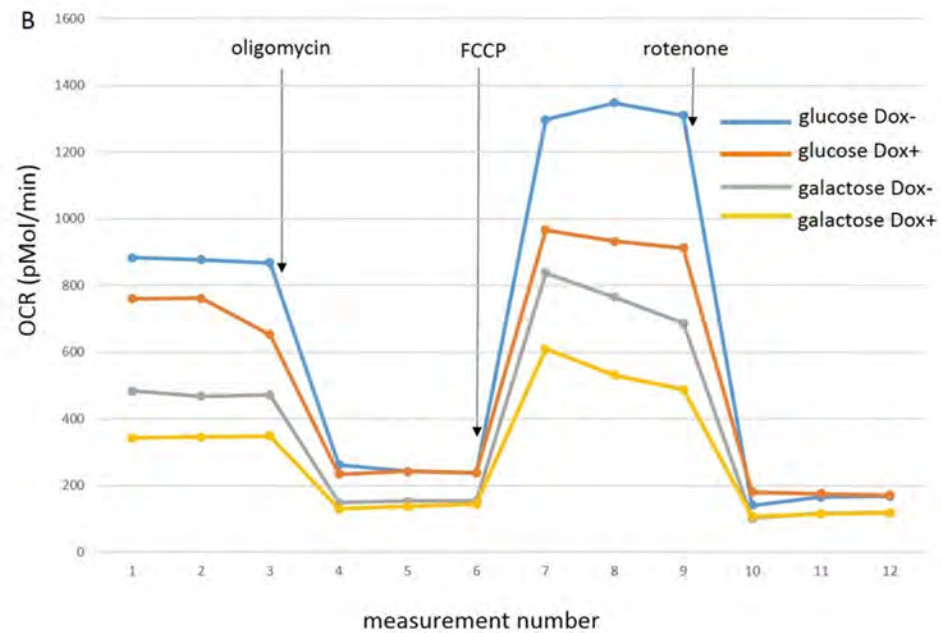
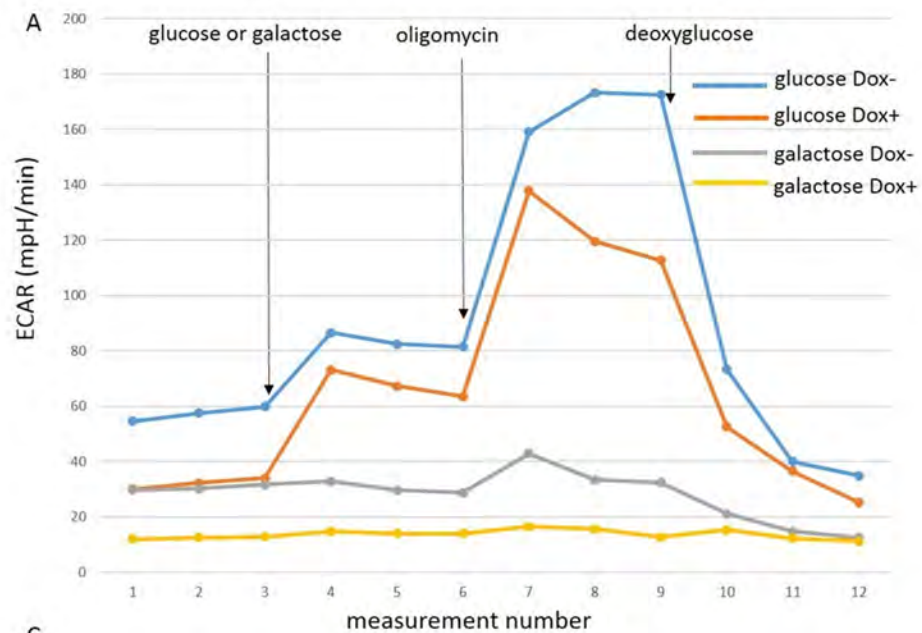


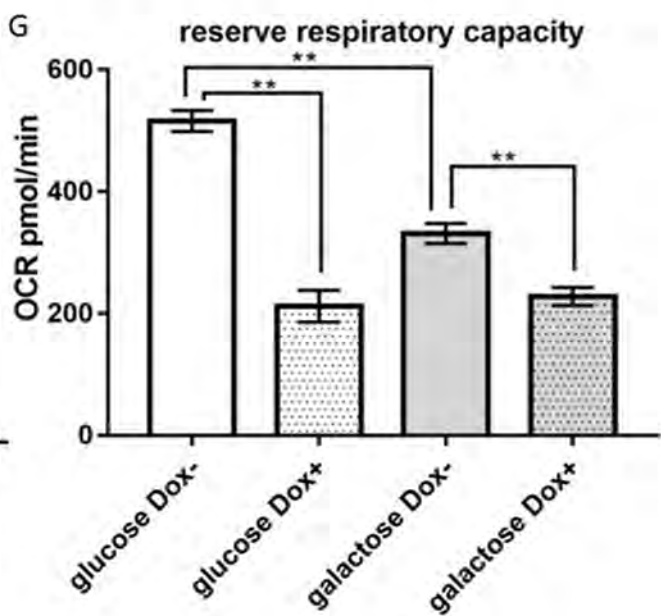
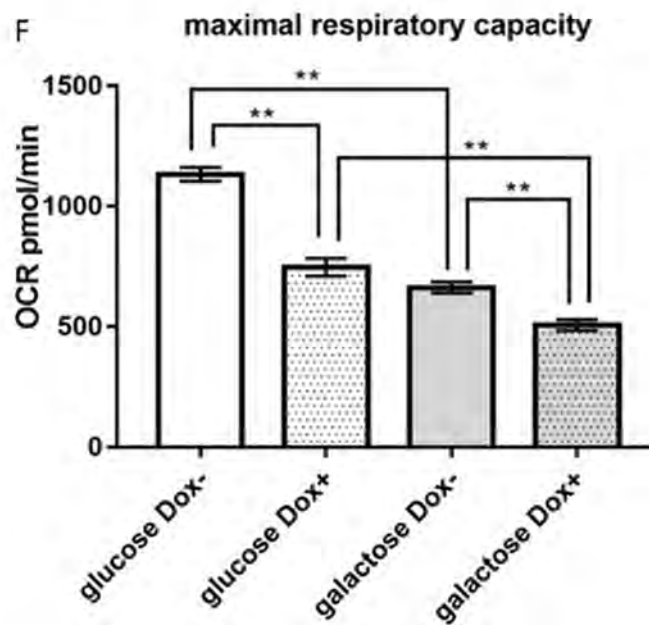
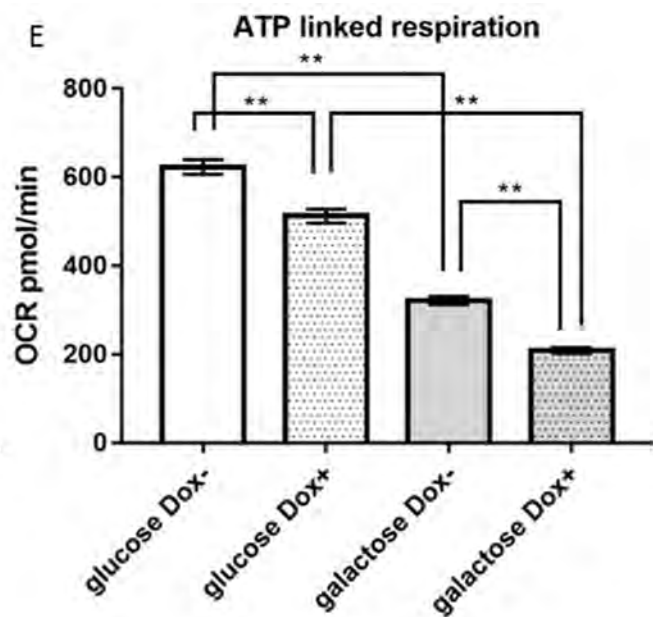
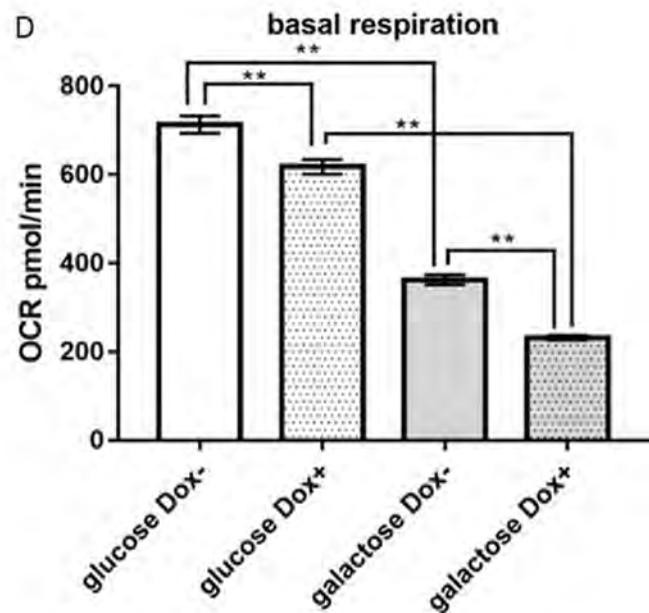
A

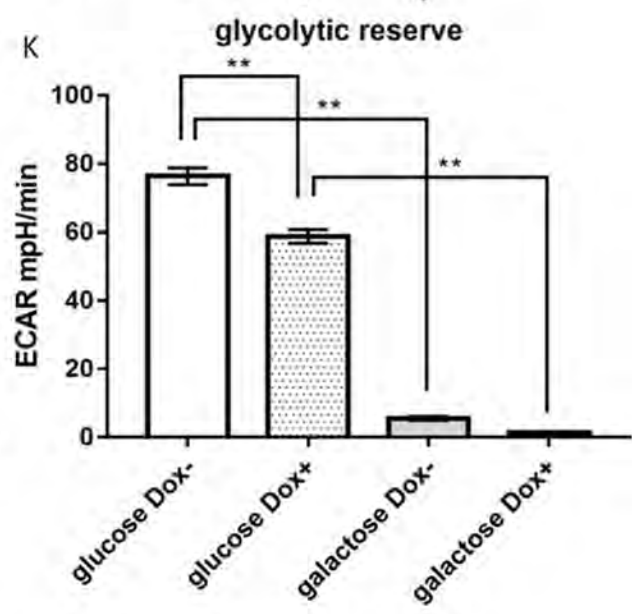
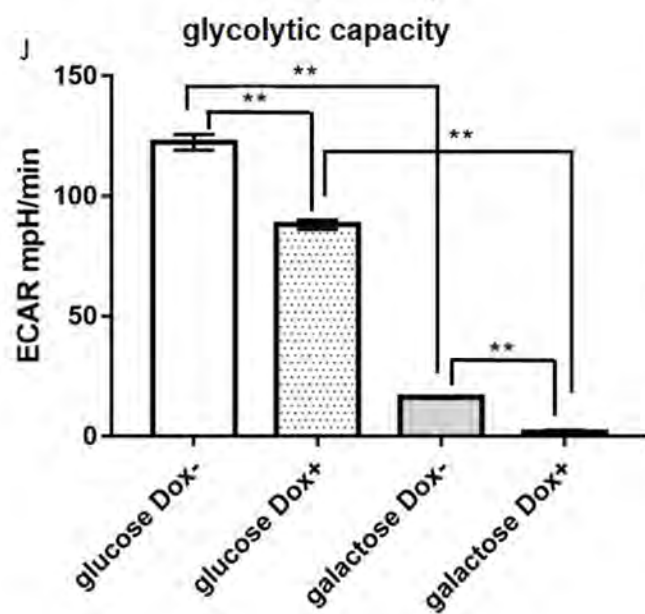
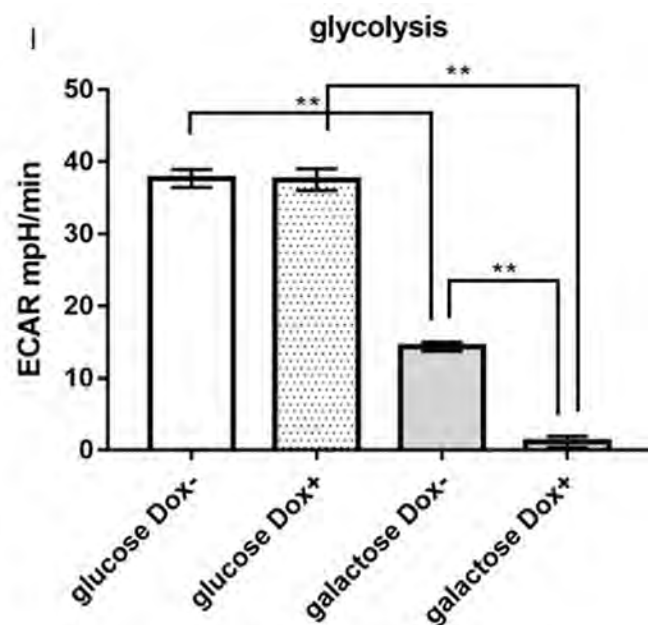
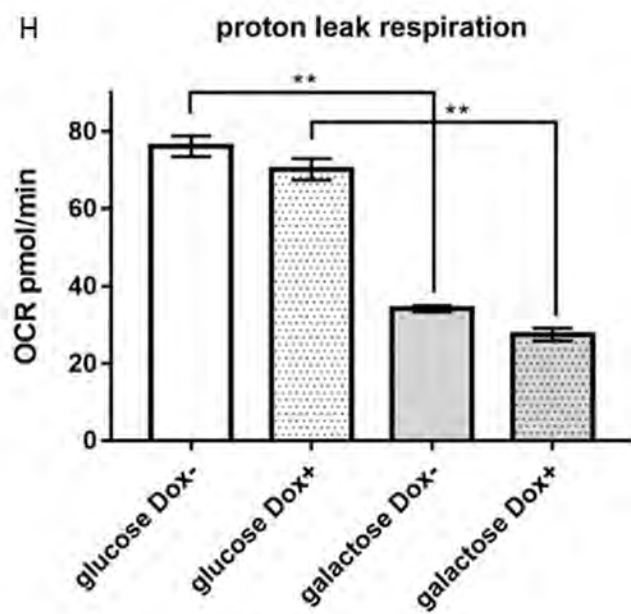


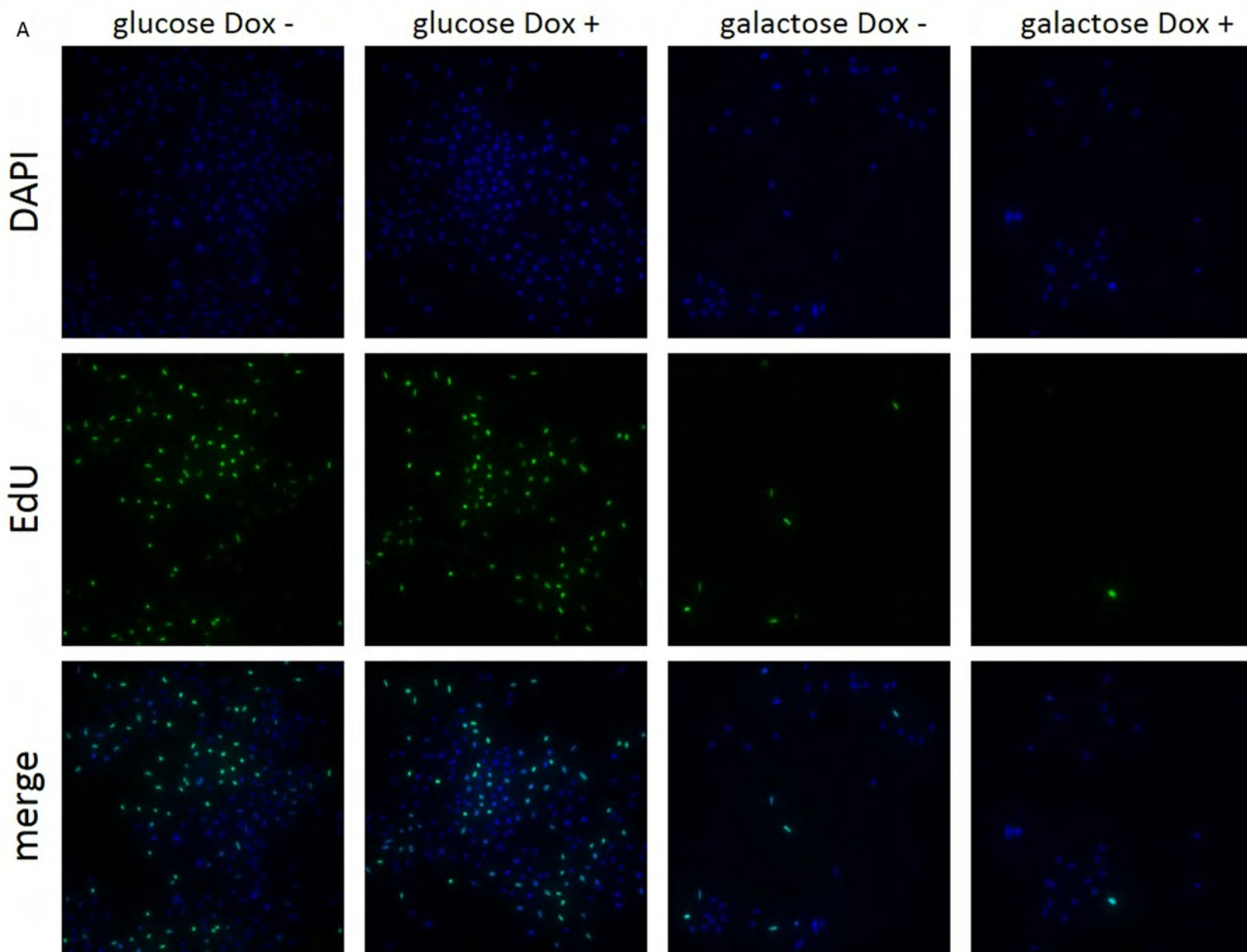
culture medium	OXPHOS subunit	OXPHOS complex
glucose	NDUFAB1	complex I
	cytochrome b-c1 subunit 1	complex III
	ATP synthase subunit $\alpha$	complex V
galactose	NDUFAF3	complex I
	cytochrome b-c1 subunit 2	complex III

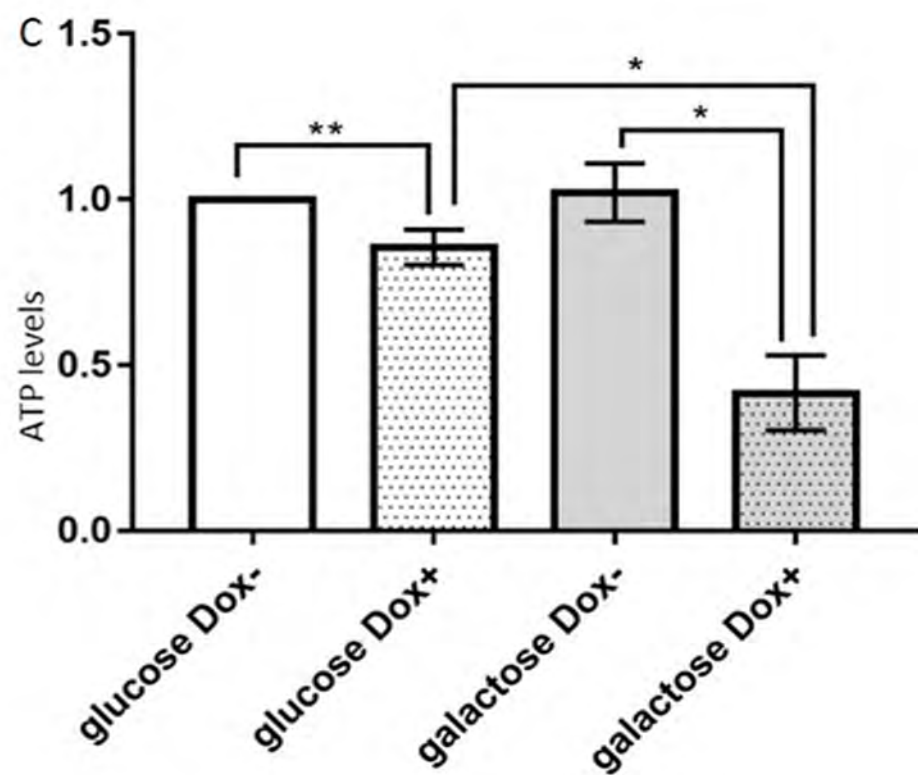
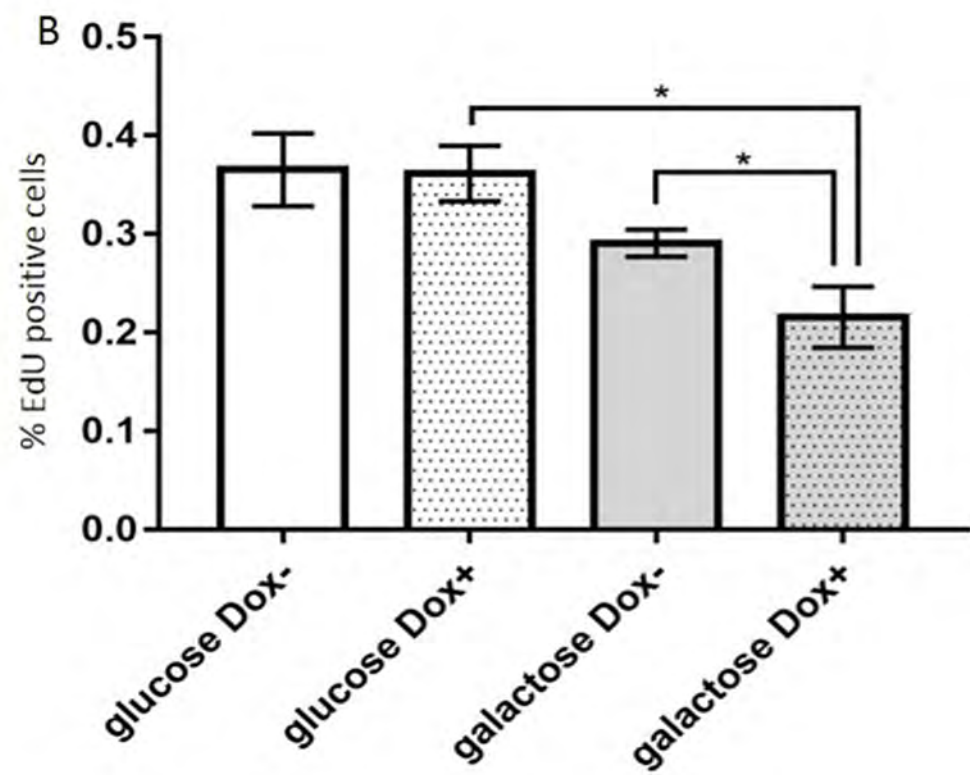












Protein spot n°	Identified protein name	Swiss-Prot accession n°	Total ion score	Sequence coverage (%)	p-value	Fold change	Identified protein function
834	acyl-CoA dehydrogenase, very long chain, mitochondrial	ACADV_HUMAN	1368	46.4	0,037	1,40	
1023	dihydrolipoyl dehydrogenase, mitochondrial	DLDH_HUMAN	847	49.7	0,00007	1,25	
1051	ATP synthase subunit alpha, mitochondrial	ATPA_HUMAN	378	22.4	0,01100	1,35	
1105	ATP synthase subunit beta, mitochondrial	ATPB_HUMAN	14519	70.7	0,03700	1,60	
1219	cytochrome b-c1 complex subunit 1, mitochondrial	QCR1_HUMAN	956	41.9	0,00140	1,20	
1357	NAD kinase 2, mitochondrial	NAKD2_HUMAN	950	54.3	0,00110	1,47	
1786	electron transfer flavoprotein subunit alpha, mitochondrial	ETFA_HUMAN	1623	70.3	0,00260	1,67	energy metabolism
1799	Delta(3,5)-Delta(2,4)-dienoyl-CoA isomerase, mitochondrial	ECH1_HUMAN	1560	60.7	0,00350	1,45	
1852	2-methoxy-6-polyprenyl-1,4-benzoquinol methylase, mitochondrial	COQ5_HUMAN	796	52.6	0,00810	1,79	
1977	enoyl-CoA hydratase, mitochondrial	ECHM_HUMAN	658	49.7	0,00300	1,57	
2051	3-hydroxyacyl-CoA dehydrogenase type-2	HCD2_HUMAN	801	70.9	0,02300	1,60	
2081	fumarate hydratase, mitochondrial	FUMH_HUMAN	632	23.1	0,00130	1,52	
2142	prostaglandin E synthase 2	PGES2_HUMAN	327	21.2	0,03700	1,58	
2744	ubiquinone oxidoreductase subunit AB1 NDUFB1, mitochondrial	ACPM_HUMAN	135	14.7	0,00560	1,72	
788	calreticulin	CALR_HUMAN	1888	64.3	0,032	1,40	
1045	cytosol aminopeptidase	AMPL_HUMAN	1746	61.3	0,01200	1,33	
1051	heat shock protein family D (Hsp60) member 1, mitochondrial	CH60_HUMAN	161	12.9	0,01100	1,35	
1215	calumenin	CALU_HUMAN	1091	56.2	0,00690	1,34	
1605	HtrA serine peptidase 2, mitochondrial	HTRA2_HUMAN	285	16.2	0,03000	1,48	
1784	pyrroline-5-carboxylate reductase 1, mitochondrial	P5CR1_HUMAN	406	27.3	0,01100	1,55	
1817	14-3-3 protein epsilon	1433E_HUMAN	1947	74.1	0,01400	1,44	quality control and stress response
1865	cathepsin D	CATD_HUMAN	827	36.7	0,01400	1,44	
2051	GrpE protein homolog 1, mitochondrial	GRPE1_HUMAN	584	49.8	0,02300	1,60	
2067	proteasome subunit alpha 5	PSA5_HUMAN	328	37.8	0,04500	1,53	
2081	glutathione S-transferase kappa 1	GSTK1_HUMAN	256	23.5	0,00130	1,52	
2142	matrix AAA peptidase interacting protein 1, mitochondrial	MAIP1_HUMAN	309	24.1	0,03700	1,58	
2364	translocon-associated protein subunit delta	SSRD_HUMAN	1075	41.6	0,01400	1,26	
1489	28S ribosomal protein S22, mitochondrial	RT22_HUMAN	1433	66.1	0,02600	1,58	
1852	prohibitin, mitochondrial	PHB_HUMAN	625	48.5	0,00810	1,79	
1888	39S ribosomal protein L28, mitochondrial	RM28_HUMAN	368	47.3	0,01200	1,43	protein biosynthesis
2067	mitochondrial assembly of ribosomal large subunit 1	MALSU1_HUMAN	309	24.8	0,04500	1,53	
2081	heterogeneous nuclear ribonucleoproteins A2/B1	ROA2_HUMAN	223	20.1	0,00130	1,52	
2081	cleavage and polyadenylation specificity factor subunit 5	CPSF5_HUMAN	212	21.1	0,00130	1,52	
1045	septin 6	SEPT6_HUMAN	481	39.4	0,01200	1,33	
1051	tubulin alpha 1a	TBB5_HUMAN	228	11.0	0,01100	1,35	cytoskeleton organization
1219	tubulin beta 4B class IVb	TBB4B_HUMAN	443	31.2	0,0014	1,20	
2260	diablo homolog, mitochondrial	DBLOH_HUMAN	694	46.9	0,02100	1,22	
2260	programmed cell death 6	PDCD6_HUMAN	725	49.2	0,02100	1,22	apoptosis
2541	histidine triad nucleotide binding protein 2, mitochondrial	HINT2_HUMAN	739	62.0	0,04400	1,43	
1020	angio-associated migratory cell protein	AAMP_HUMAN	604	36.6	0,02500	1,35	
1740	voltage dependent anion channel 1, mitochondrial	VDAC1_HUMAN	3028	70.0	0,04900	1,35	other
2051	growth factor receptor-bound protein 2	GRB2_HUMAN	604	68.2	0,02300	1,60	
2161	cell division control protein 42 homolog	CDC42_HUMAN	195	38.2	0,02400	2,15	

Protein spot n°	Identified protein name	Swiss-Prot accession n°	Total ion score	Sequence coverage (%)	p-value	Fold change	Identified protein function
209	carbamoyl-phosphate synthase 1, mitochondrial	CPS1_HUMAN	295	7.6	0,0039	-1,30	
231	ATP-citrate synthase	ACLY_HUMAN	685	21.3	0,0100	-1,80	
370	Cytoplasmic aconitate hydratase	ACOC_HUMAN	111	3.6	0,0045	-1,37	
525	ATP-dependent 6-phosphofructokinase	PFKAP_HUMAN	763	31.4	0,026	-1,45	
1192	gamma-enolase	ENOG_HUMAN	2107	74.7	0,0310	-1,59	
1236	alpha-enolase	ENOA_HUMAN	847	43.1	0,0040	-1,50	energy metabolism
1360	phosphoglycerate kinase 1	PGK1_HUMAN	1409	72.2	0,0490	-1,54	
1479	farnesyl pyrophosphate synthase	FPPS_HUMAN	599	33.7	0,0250	-2,30	
1577	glyceraldehyde-3-phosphate dehydrogenase	G3P_HUMAN	337	76.3	0,0080	-1,30	
1972	protein ABHD11	ABHDB_HUMAN	483	35.6	0,0200	-1,38	
1972	phosphoglycerate mutase 1	PGAM1_HUMAN	356	57.5	0,0200	-1,38	
447	heat shock protein HSP 90-beta	HS90B_HUMAN	383	15.6	0,03	-1,32	
748	heat shock 70 kDa protein 1A	HS71A_HUMAN	2339	61.9	0,0120	-1,31	
787	T-complex protein 1 subunit gamma	TCPG_HUMAN	2158	66.2	0,0074	-1,31	quality control and stress response
962	T-complex protein 1 subunit eta	TCPH_HUMAN	2655	68.9	0,0036	-1,26	
1059	T-complex protein 1 subunit beta	TCPB_HUMAN	5746	76.8	0,0086	-1,36	
1236	DnaJ homolog subfamily A member 1	DNJA1_HUMAN	1912	62.2	0,0040	-1,50	
369	elongation factor 2	EF2_HUMAN	2074	46.5	0,0240	-1,34	
436	pre-mRNA-splicing factor ATP-dependent RNA helicase DHX15	DHX15_HUMAN	513	18.4	0,019	-1,53	protein biosynthesis
787	heterogeneous nuclear ribonucleoprotein Q	HNRPO_HUMAN	660	33.4	0,0063	-1,32	
787	far upstream element-binding protein 1	FUBP1_HUMAN	588	27.5	0,0063	-1,32	
203	vinculin	VINC_HUMAN	649	17.6	0,0039	-1,30	
447	cortactin	SRC8_HUMAN	1006	42.9	0,03	-1,32	
644	moesin	MOES_HUMAN	558	35.5	0,044	-1,80	cytoskeleton organization
785	plastin-3	PLST_HUMAN	1751	58.4	0,0066	-1,44	
1004	adenylyl cyclase-associated protein 1	CAP1_HUMAN	1124	45,9	0,0230	-1,27	
239	importin-5	IPO5_HUMAN	2303	39,9	0,0045	-1,56	
644	dynamitin 1 like	DNM1L_HUMAN	411	18,9	0,044	-1,80	
644	lamin A/C	LMNA_HUMAN	884	31,0	0,044	-1,80	
1291	adenosylhomocysteinase	SAHH_HUMAN	1215	39,6	0,0160	-1,30	
1547	serine/threonine-protein phosphatase PP1-beta catalytic subunit	PP1B_HUMAN	889	64,2	0,0080	-1,30	other
1547	annexin A1	ANXA1_HUMAN	654	45,4	0,0080	-1,30	
1907	chloride intracellular channel 4	CLIC4_HUMAN	1683	76,0	0,0460	-1,60	
1972	hydroxyacylglutathione hydrolase, mitochondrial	GLO2_HUMAN	224	24,0	0,0200	-1,38	
2690	barrier to autointegration factor 1	BAF_HUMAN	81	40,4	0,028	-1,47	

Protein spot n°	Identified protein name	Swiss-Prot accession n°	Total ion score	Sequence coverage (%)	p-value	Fold change	Identified protein function
872	bifunctional coenzyme A synthase	COASY_HUMAN	497	24.1	0,021	1,19	energy metabolism
872	electron transfer flavoprotein-ubiquinone oxidoreductase, mitochondrial	ETFD_HUMAN	1043	43.1	0,021	1,19	
1295	cytochrome b-c1 complex subunit 2, mitochondrial	QCR2_HUMAN	424	29.4	0,017	1,31	
1321	succinyl-CoA ligase ADP-forming subunit beta, mitochondrial	SUCB1_HUMAN	963	47.1	0,013	1,33	
1349	medium-chain specific acyl-CoA dehydrogenase, mitochondrial	ACADM_HUMAN	787	40.9	0,029	1,34	
1899	protein ABHD11	ABHDB_HUMAN	262	31.4	0,017	1,17	
2142	prostaglandin E synthase 2	PGES2_HUMAN	327	21.2	0,046	1,48	
305	DNA mismatch repair protein Msh2	MSH2_HUMAN	875	30.0	0,011	1,35	quality control and stress response
1592	AH receptor interacting protein	AIP_HUMAN	359	46.7	0,022	1,33	
1605	HtrA serine peptidase 2, mitochondrial	HTRA2_HUMAN	285	16.2	0,011	1,39	
1865	cathepsin D	CATD_HUMAN	827	36.7	0,013	1,52	
1876	T-complex protein 1 subunit beta	TCPB_HUMAN	781	37.9	0,017	1,18	
2142	matrix AAA peptidase interacting protein 1, mitochondrial	MAIP1_HUMAN	309	24.1	0,046	1,48	
1865	14-3-3 protein epsilon	1433E_HUMAN	406	43.1	0,013	1,52	
2855	ubiquitin-40S ribosomal protein S27a	RS27A_HUMAN	117	67.6	0,023	1,31	protein biosynthesis
305	alanine--tRNA ligase, mitochondrial	SYAM_HUMAN	649	25.4	0,011	1,35	
801	X-ray repair cross complementing 6	XRCC6_HUMAN	176	12.2	0,0019	1,32	
1295	flap endonuclease 1	FEN1_HUMAN	389	30.0	0,017	1,31	
1443	eukaryotic translation initiation factor 3 subunit H	EIF3H_HUMAN	1120	59.7	0,0069	1,16	
1474	heterogeneous nuclear ribonucleoproteins C1/C2	HNRPC_HUMAN	164	19.9	0,003	1,82	
1474	serine-threonine kinase receptor-associated protein	STRAP_HUMAN	120	11.7	0,003	1,82	
1489	28S ribosomal protein S22, mitochondrial	RT22_HUMAN	1433	66.1	0,042	1,34	other
1734	prohibitin-2	PHB2_HUMAN	1743	69.2	0,025	1,29	
2152	heterogeneous nuclear ribonucleoprotein A1	ROA1_HUMAN	1129	33.3	0,039	1,87	
1605	ribose-phosphate pyrophosphokinase 2	PRPS2_HUMAN	317	25.5	0,011	1,39	
1321	lamin A/C	LMNA_HUMAN	617	27.4	0,013	1,33	
1326	actin, cytoplasmic 1	ACTB_HUMAN	1437	61.1	0,0055	1,46	
1592	annexin A2	ANXA2_HUMAN	802	45.7	0,022	1,33	
1605	3-mercaptopyruvate sulfurtransferase	THTM_HUMAN	630	48.1	0,011	1,39	
1737	annexin A5	ANXA5_HUMAN	666	53.8	0,0019	1,32	
1865	chloride intracellular channel 2	CLIC2_HUMAN	476	56.0	0,013	1,52	



Protein spot n°	Identified protein name	Swiss-Prot accession n°	Total ion score	Sequence coverage (%)	p-value	Fold change	Identified protein function
89	carbamoyl-phosphate synthase ammonia, mitochondrial	CPS1_HUMAN	3560	53.3	0,018	-1,44	
276	neutral alpha-glucosidase AB	GANAB_HUMAN	1361	37.8	0,00087	-1,8	
1192	gamma-enolase	ENOG_HUMAN	2107	74.7	0,025	-1,32	
1360	phosphoglycerate kinase 1	PGK1_HUMAN	3151	75.8	0,025	-1,23	energy metabolism
1360	fructose-bisphosphate aldolase A	ALDOA_HUMAN	1160	74.2	0,025	-1,23	
1360	glyceraldehyde-3-phosphate dehydrogenase	G3P_HUMAN	132	8.4	0,025	-1,23	
2409	NADH dehydrogenase ubiquinone 1 alpha subcomplex assembly factor	NDUF3_HUMAN	234	25.0	0,038	-1,36	
304	heat shock protein HSP 90-beta	HS90B_HUMAN	76	3.2	0,035	-1,46	
1425	ubiquitin domain-containing protein UBFD1	UBFD1_HUMAN	730	42.1	0,013	-1,27	quality control
1425	26S proteasome non-ATPase regulatory subunit 13	PSD13_HUMAN	319	33.0	0,013	-1,27	and stress response
2409	prefoldin subunit 5	PF5_HUMAN	285	43.5	0,038	-1,36	
1482	glutaredoxin-3	GLRX3_HUMAN	312	37,6	0,017	-1,81	
584	radixin	RADI_HUMAN	1290	52.0	0,019	-1,45	
1360	calcium uptake protein 2, mitochondrial	MICU2_HUMAN	346	20.0	0,025	-1,23	
1482	guanine nucleotide-binding protein G(i) subunit alpha-2	GNAI2_HUMAN	1222	62,3	0,017	-1,81	
2252	ferritin light chain	FRIL_HUMAN	1451	50.3	0,036	-1,29	other
2351	eukaryotic translation initiation factor 1A, X-chromosomal	IF1AX_HUMAN	329	43.1	0,0089	-1,72	
2351	exosome complex component RRP4	EXOS2_HUMAN	201	20.5	0,0089	-1,72	
2586	galectin 1	LEG1_HUMAN	693	73.3	0,043	-1,44	